INNOVATIVE VIBRATION TECHNIQUE AS A VIABLE SUBSTITUTE FOR CONVENTIONAL THREE POINT BENDING FATIGUE TESTING

By

Alexander Peralta Serrano

A thesis submitted in partial fulfillment of the requirements for the degree of

MASTER OF SCIENCES
in
MECHANICAL ENGINEERING

UNIVERSITY OF PUERTO RICO
MAYAGÜEZ CAMPUS
2008

Approved by:

Abdul Basir Shafiq, PhD Member, Graduate Committee	Date
David Serrano, ScD Member, Graduate Committee	Date
Frederick Just A., PhD President, Graduate Committee	Date
Paul Castillo, PhD Representative of Graduate Studies	Date
Paul Sundaram, PhD Chairperson of the Department	Date

ABSTRACT

Fatigue lifetime prediction of various materials under three-point-bending is generally limited to the long testing periods consumed and the economic inversion needed develop the test. The use of a vibration technique as a possible alternative to predict fatigue life can be an attractive cost effect option. An innovative vibration fatigue methodology is developed. The procedure uses geometric shape optimization along with finite element analysis to ensure that a specific three-point-bending stress pattern is mimicked in a given region of the test specimen while vibrating in the first resonance. The methodology was compared with three-point-bending tests for two different materials: FR-7140 foam and a sandwich composite. When compared to three-point-bending tests results, the vibration technique showed to be very promising and lifetime predictions fell clearly within the ninety percent confidence levels of the three-point-bending tests.

RESUMEN

La predicción del tiempo de vida en fatiga de diversos materiales, bajo la configuración de T.P.B. generalmente es limitado por su alto consumo de tiempo e inversión económica durante su desarrollo. Utilizar el concepto de vibraciones, como posible alternativa para predicción de vida en fatiga, se convierte en una opción atrayente, por la ventaja que ofrecen en el significativo ahorro de tiempo y dinero durante el desarrollo de sus pruebas. Este trabajo desarrolla una innovativa técnica de fatiga, utilizando vibraciones; valiéndose de las propiedades modales de los materiales y utilizando optimización geométrica de los especimenes. En esta técnica, el patrón de esfuerzos generados por vibraciones busca imitar la distribución de esfuerzos generados en los especimenes por T.P.B. y fue aplicada en dos materiales, foam FR-7140 y materiales Compuestos Sándwich, obteniendo resultados experimentales muy razonables comparados con los obtenidos por T.P.B.

TO MY FAMILY…

Acknowledgments

To God and my Family for support me in throughout of my life, also I would like to thank my advisor, Dr. Just Frederick A. by his constant guidance and support throughout this research, finally I thank Drs. Shafiq Abdul Basir and David Serrano, for their help and good disposition.

TABLE OF CONTENT

List of Tables

List of Figures

CHAPTER 1

1. INTRODUCTION

Structures constructed with sandwich composites can offer a very high rigidity to weight ratio increased used applications ranging from satellites, aircraft, automobiles, rail cars, wind energy systems, bridge construction, and marine vessels continues to grow. A sandwich composite is usually structured of two face sheets and a core as depicted in Figure 1.1. This construction does not have to be symmetric and the sandwich can have multiple cores within the face sheets. The core material is normally a low strength material and provides the sandwich composite with transverse stiffness; face sheets on the other hand give the material the bending resistance needed. Sandwich composites can be constructed with a variety of face sheet and core materials. Common core materials can range from balsa, polyurethane foam, honeycomb craft paper, aluminum foam or even truss configurations to name a few. Face sheets can be a variety of material these can include metal, wood, fiber reinforced materials with either a polyester resign or epoxy matrix.

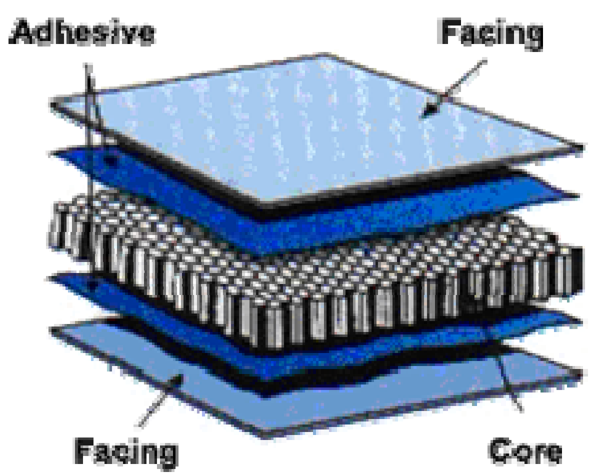

Figure 1.1: Sandwich composite structure

Because of the many advantages and the increased use of sandwich composite construction, knowledge of their behavior and loading properties must be known.

This proposal will suggest future research on a vibration fatigue methodology to determine the fatigue behavior of sandwich composites.

OBJECTIVES

The main objective of this research is to develop a novel methodology that can be used to determine the characteristic fatigue life of sandwich composite materials using a vibration technique. The technique will be able to reduce the time in fatigue testing by an order of magnitude which in turn will have significant savings in money. Here a procedure to design the test specimen will be developed. The specimen, when tested at a fixed frequency, should produce a deflection pattern that will mimic typical fatigue testing In order to develop this technique mathematical modeling, finite element analysis, shape optimization, and experimental real-time mode shape calculations will be implemented.

JUSTIFICATION:

The need for fatigue characterization of sandwich composites is clearly evident. Advances in the use of sandwich composites as structural materials can be found in many applications such as transportation, marine vessels, tanks, refrigerator containers, bridge decks and even car body shells to name a few. In these applications the high strength to weight ratio of this material offers an attractive solution. In typical applications, these structures are often subjected to repetitive loading that may lead to fatigue failure, for example the effect of sea waves striking the hull of a marine vessel during its lifetime.

This cyclic loading can limit the life of the sandwich composite material and even alter its properties.

Several methodologies for impact and fatigue testing exist. Current fatigue testing is usually performed on hydraulic servo machines operating in the 1-10 Hz frequency range. In order to obtain one point in a S-N diagram for 10^6 cycles of testing, at a frequency of 10Hz, a period of around 28 hrs is needed. If the structure endures 10^7 cycles around 12 days are required to test one point. The typical suggested test procedure for an S-N-P diagram requires around 4 to 5 data points in the diagram. Each data point is usually determined using the average of 15 specimens tested at a given frequency and stress ratio. If testing is charged at the rate of one dollar per hour, a typical test could cost between $17,280 to 21,600 dollars per material configuration. The ability to develop a test procedure that can operate at higher frequencies can reduce cost significantly. If the rate of testing is increased by ten fold costs would now range from $1,728 to $2,160 per material configuration, a savings of around over $15,000!

METHODOLOGY

The procedure used to design the vibration test specimen will consist of several phases. Basically, a specimen will be designed to operate in resonance producing a mode shape that will mimic the deflection profile used in typical fatigue testing. Modeling will consist of developing the governing equations of the specimen during vibration and then performing Finite Element Analysis to determine the mode shapes and frequencies. Because the natural frequency and mode shape are highly dependent upon the material properties and geometry of the specimen under question, a shape optimization procedure will be used to vary these parameters until the desired vibration profile and frequency are determined. This procedure is outlined in Figure 1.2. After the shape optimization is performed validation of the procedure will be done with experimental vibrations. An electromechanical shaker will be used to excite the structure. Several sensors located at different positions along the span of the specimen will be used to monitor the translational mode shapes. Curvature variation of the mode shape will determine when fatigue damage has occurred.

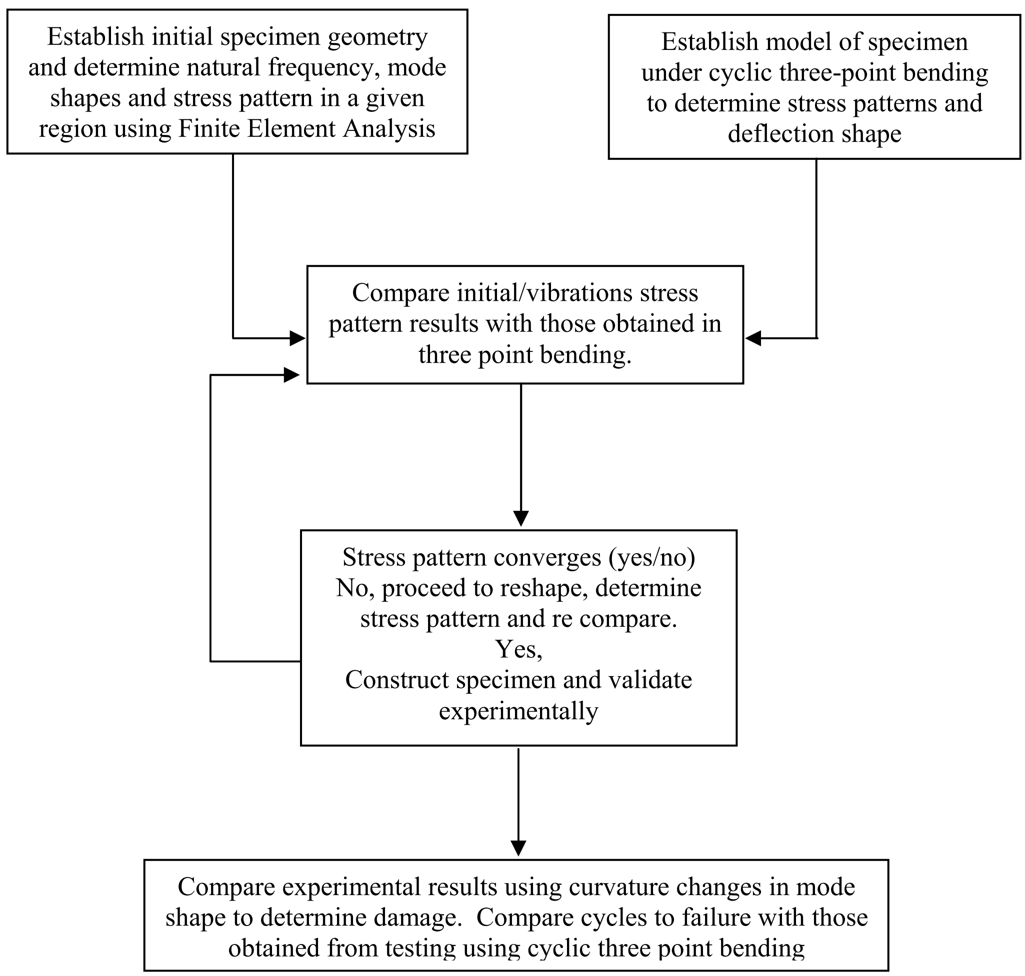

Figure 1.2: Outline of procedure used in specimen design and testing

CHAPTER 2

LITERATURE REVIEW

Sandwich composite testing can be performed using many different methods that yield different aspects of the material properties. These testing methodologies can include areas such as: non-destructive evaluation, environmental factors, failure modes with analytical modeling and even testing procedures to name a few. Unfortunately, the literature available is primarily concentrated on fiber matrix configurations and currently there is a limited amount of work on sandwich composites especially in the area of fatigue behavior. The following literature review will cover some of the areas mentioned above with a focus on sandwich composite materials.

2.1 FAILURE MODES

Structural failure of sandwich composites can be attributed to many factors: ranging from loading, aging and even the operational environment. In addition these modes can be classified in many different ways that can include loading effects such as tension or compression failure of the facings, shear failure of the core, wrinkling failure of the compression facing, local indentation, debonding of the core/facing interface, and global buckling to name a few. Usually the initiation, propagation, and interaction of failure modes depends a great deal on the type of loading, constituent material properties, and geometrical dimensions. Hence, this section of the literature review will examine literature related to the various failure modes that occur in sandwich composites under static loading, impact loading, and fatigue loading.

2.1.1 Static Loading

Several investigations studying the basic failure modes of sandwich composites under static loading have been published by various authors: Allen [1] and Zenkert [2], Daniel et al. [3], Gdoutos et al. [4, 5], Steeves and Fleck [6, 7]. In addition, Lee and Tsotsis [8] investigated indentation failure in honeycomb panels and Pan et al. [9] studied the shear failure process in honeycomb cores in sandwich structures.

Petras and Sutcliffe [10] developed failure mode maps for honeycomb sandwich beams with specimens made from GFRP laminate skins and Nomex honeycomb cores. Three-point bend tests were carried out using the ASTM C393-62 [11] standard. Observed failure modes were divided into two categories: skin failure (that included face yielding, intra-cell dimpling and face wrinkling) and core failure.

2.1.2 Impact loading

In addition to static loading, impact testing on sandwich composites has also been investigated. Lim et al [12] studied the transverse impact failure modes in foam core sandwich beams. Impact tests using the ASTM D 5942 standard [13] were performed on specimens with various and facesheet and core density configurations. Abrate [14], [15] also examined the similar type specimens. In both cases impact loading induced damage to the facings, the core material, and the core–facing interface.

Todd A. Anderson, [16] researched the effect of impact duration and classified the impact with respect to period of the first natural frequency of the specimen. Impacts having a duration significantly longer than the period of the lowest natural frequency of the structure were termed low velocity impacts. These types of collisions usually occur when a large mass strikes an object. Impacts classified under this category were found to initiate internal damage that is difficult or impossible to detect from the exterior face sheet surface of foam and honeycomb sandwich structures.

Analytical and computational and experimental studies were also performed to predict and characterize the damage created by wave propagation and boundary condition controlled impacts. Here the stiffness parameters of the models were derived from experimental results using energy-dissipating elements that were incorporated into the models to account for material damage. Model validity was examined with comparisons of experimental force histories resulting from impact on six different core and face sheet configurations.

2.1.3 Fatigue loading

Failure modes found in fatigue loading are often similar to those observed in static and impact loading. Harte et al [17] investigated cyclic loading of sandwich beams with aluminum alloy foam. Three failure modes were observed: face-sheet yield, core shear, and indentation. Kulkarni et al [18] studied fatigue failure mechanisms in sandwich beams made of glass/epoxy and PVC foam. Sandwich panels were manufactured using the co-injection resin transfer molding (CIRTM) process to infuse the resin simultaneously in both top and bottom face sheets. Fatigue tests were carried out in three-point bending. Results concluded that the predominant failure mode in cyclic fatigue loading was initiated with core shear. Here the complete core shear crack growth mechanism was studied, damage in the core was analyzed at a microscopic level and the crack growth mechanism was investigated.

In most of the fatigue testing work performed in laboratories involves constant amplitude sinusoidal loading using three-point or four-point bend tests. But composite structures are rarely subjected to uniform constant amplitude service loads. Loads usually fluctuate randomly producing a load spectrum in addition; the load can vary in sequential steps (i.e., block amplitude loading) or even consist of various combinations of these types of loading.

Very little work has been performed using block loading on sandwich structures. Gamstedt and Sjogren [19] studied about the sequence effect in block amplitude loading for carbon-fiber /epoxy cross-ply laminates, as results they obtained that a sequence of high-low amplitude levels results in shorter lifetimes than low-high order amplitudes. Clark et al [20] investigated the fatigue behavior of sandwich beams using a two-step block-loading regimen. Sandwich samples used a Airex C70.130 thermoset cross-linked cellular foam, with face sheets manufactured with a hybrid glass/Kevlar/epoxy balanced 0/90 woven construction. A combination of low–high loads and then high–low loads were investigated. Beams were loaded with fifty percent of their average fatigue life at each respective load. Most of the beams did not fail and were tested for their residual static strength under static loading conditions. Results concluded that under two-step loading no fatigue failures occurred, thus producing a stronger sample as compared to those used in single loading tests.

2.2 EFFECT OF ENVIRONMENTAL FACTORS

Sandwich composites are used in a vast range of environments ranging from Nordic to topical environments. Temperature and moisture have been reported to vary material properties significantly. The effect of temperature on the behavior on fracture toughness and fatigue life of sandwich composites using constituents of Nomex honeycomb core with graphite/epoxy skins was investigated by Berkonitz and Johnson [21]. Here specimens were tested with a double cantilever beam configuration using the ASTM D5528-94a code as a guideline for the fracture toughness testing. The experiments were evaluated using a displacement control mode at a frequency of 4-Hz with a R-ratio (Pmin/Pmax) of 0.1 in under three temperature conditions: a hot temperature, a cold temperature and room temperature. Results showed that fracture toughness was inversely proportional to temperature; the lower the temperature, the higher the fracture toughness.

In addition to fatrue toughness tesing the effect of temperature on impact has been investigated by Erickson et al [22]. Here the effect of temperature on the low velocity impact of composite sandwich panels was investigated. Sandwich panels were manufactured with a cross-woven E-glass 0/90 weave in an epoxy matrix. Four different core material-thickness combinations were used these consisted of a 2.54 and 1.43 cm thick cardboard honeycomb core filled with a low density foam and a 2.54 and 1.43 cm thick plain cardboard honeycomb. The impact tests were carried out at three different temperatures. Specimens tested at low temperature exhibited back face sheet delamination. Samples tested at room temperature showed fiber breakage and delamination on the back face sheet and high temperature samples were completely penetrated.

Kanny and Mahfuz et al [23] investigated the effects of elevated temperature on the fatigue behavior of foam core sandwich structures. Sandwich specimens using two types of PVC cores: High-density foam and cross-linked high-density foam, having face sheets made of glass/vinyl ester composite were tested under three-point bending. Static tests showed that the strength of the sandwich beams decreased with an increase in temperature. Close inspection revealed that damage occurred mainly in the foam cores and was more severe in high-density beams.

In addition to changing temperature environments, sandwich structures used in marine applications are exposed to seawater for long periods of time. Smith and Weitsman [24] investigated the immersed fatigue response of polymer composites. Results showed that fatigue life was reduced drastically when saturated specimens were fatigued in an immersed environment. In addition, Weitsman and Elahi 35 also published a review article on the effects of fluids on deformation, strength, and durability of polymeric composites that showed similar results.

2.3 ANALYTICAL MODELING

Analytical modeling used in the study of fatigue mechanisms in sandwich composites testing is limited. Most studies include the use of fatigue loading S-N modeling, strength degradation classification, stiffness reduction and commutative damage modeling.

2.3.1 Basic S-N approach

Kanny K and Mahfuz [25], and Burman M. and Zenkert [26,27] have performed work on lifetime prediction using S-N curves for sandwich composites. Kanny and Mahfuz [25] investigated flexural fatigue tests performed on sandwich beams made up of a glass fiber skin and polyvinyl chloride (PVC) core of varying densities and derived a simple expression for predicting the fatigue life of foam core sandwich beams. The approach used an empirical expression that best fitted the S-N curve for the given material. . Burman and Zenker [26,27] also proposed a simple curve fitting S-N approach using a two-parameter Weibull function. Reasonable agreement between experimental and analytical results was obtained.

2.3.2 Strength degradation approach

The Strength degradation approach examines characterizes the strength reduction that occurs in a material during fatigue life testing. A review of various residual strength degradation fatigue theories for composite materials was performed Sendeckyj [28]. Dai and Hahn [29] developed a wear-out model for sandwich beams. This work assessed the fatigue behaviors of sandwich beams using the concept of strength degradation. The model requires only two parameters to describe the strength degradation in fatigue. One parameter represents the rate of the degradation; the other the relative fatigue life. Dai and Hahn [29] also proposed a new approach to determine the degradation that predicted fatigue using three parameters: the fatigue stress, the residual strength, and the number of cycles applied, respectively.

2.3.3 Stiffness Reduction Approach

Reifsnider et al [30], Wu, Lee and Choy, et al [31] performed research that used the residual stiffness technique as a parameter to describe degradation behavior in predicting fatigue life. This methodology was perfered because the residual stiffness can be monitored nondestructively and therefore can de related to the residual strength and fatigue life of the specimen. In addition, El Mahi et al [32] also developed a model-based method using the stiffness reduction approach for sandwich composites. Results were compared with experimental data from three-point bending fatigue tests on specimens made with PVC foam core and E-glass/epoxy skins.

2.3.4 Cumulative Damage Modeling

Several authors have used a modified Palmgren–Miner [33] model for composites materials. Sendeckyj [28] reviewed fatigue accumulation models and compared the applicability and accuracy of each model, including the life prediction models proposed by Hashin and Rotem [34], Wang et al [35], and Broutman and Sahu [36]. More recently, Epaarachchi and Clausen [37] have also developed a new cumulative damage model for glass fiber-reinforced plastic (GFRP) composites. All of these models are specifically for composite laminates, which can be used as skins in sandwich structures. By contrast, there seem to be few publications on the use of cumulative damage models for composite sandwich materials. Clark et al [20] reported on cumulative damage modeling of sandwich beams based with the stiffness degradation approach under two-step loading.

2.4 NONDESTRUCTIVE EVALUATION (NDE)

Sandwich structures and materials exhibit different modes of failure, each of which may have a different NDE signature. In fatigue testing, damage initiation and propagation is extremely important during testing. In general, there is no single NDE method that will adequately cover all aspects of fatigue damage, and in most cases a combination of various NDE methods is necessary for complete characterization of a specific type of damage.

2.4.1 Ultrasonic methods

Ultrasonic investigation ranging from using C-scan testing in foams to even wavelet analysis with this NDE evaluation method has been performed. Sachse et al [38] reviewed work in the area of quantitative ultrasonic NDE, and summarized new approaches for active and passive methods in composite materials measurements. In the area of C-scans, Akay and Hanna [39] assessed damage in Nomex honeycomb and Roacell foams and Gupta and Sankaran [40] investigated foam quality and skin/core debonds. In addition, Legendre, Goyette, and Massicot et al [41], have utilized wavelets in ultrasonic NDE evaluation of composite materials.

2.4.2 Infrared/ Thermal wave methods

In addition to the use of Ultrasonic methods, Infrared (IR) thermography NDE has also been used on composite materials. IR thermal wave analysis was performed Favro et al [42,43] for wide-area inspection of structures. Inspection of new aero engines with thermal wave thermography and the use of thermal waves to acquire color-coded temperature profiles were performed by Guazzone and Danjoux [44] and Dattoma et al [45] respectively. In all cases, the authors asserted the impossibility of using thermal waves to capture accurate dimensions of defects, and its suitability of the method as a good complementary technique to other NDE approaches. A method to eliminate surface roughness effects using a spatial white noise description in thermal wave NDE identification and its potential in many practial applications was performed by Mandelis [46]. In addition, Mandelis, Munidasa, and Nicolaides [47] applied laser infrared photothermal radiometry to various thermal wave inverse-problem NDE applications.

2.4.3 Vibration Methods

Vibration nondestructive analysis usually involves impulsive, random or sine sweep excitation of a test specimen upon which Fast Fourier Transform analysis of the response is performed. Here identification of modal frequencies, damping and mode shapes can be combined with analytical modeling to determine intrinsic properties of the specimen under test. Material or geometric changes due to degradation usually result in corresponding changes in the modal parameters.

A summary of recent work used modal vibration response measurements in characterizing composite materials and structures was performed by Gibson [48]. Liew, Xiang, and Kitiponchai [49] reviewed vibration work on thick composite plates, Salawu [50] summarized vibration based damage detection that focused on frequency change methods. The used of vibration NDE to evaluate impact damage of sandwich composite structures reinforced in the thickness direction was performed by Palozotto et al. [51]. In addition, Ayorinde [52], employed an inverse method based on a Timoshenko–Mindlin formulation to develop a method for the elastic characterization of thick composite plates. Free-vibration of sandwich beams with simple and double delaminations has been investigated by Shu, [53]. Solutions to the governing equations were express in analytical form without resorting to numerical approximations. Modeling was performed with an Euler-Bernoulli approximation to determine the vibration mode shapes along with the local deformations at the delaminating fronts. The validity of these assumed geometry and boundary conditions were compared with experimental results. The solution for double delaminations resulted in both higher modes and mixed modes vibrations revealing a multitude of natural frequencies within a narrow range.

2.5 OTHER RELATED WORKS

Tommy George, Jeremy Seidt, Hernan Shen, Theodore Nicholas and Charles J. Cross, O. Scott-Emuakpor [54], [55] and [56] investigated a testing methodology to determine the fatigue limit strength of structural materials at high frequencies. The procedure involved a base-exited plate specimen driven into a high frequency resonant mode which allows completion of a fatigue test in a few hours. Specimen design consisted in using a topological design procedure, incorporating a finite element model, to produce its shape. Only steel, 6061-T6 aluminum and Ti-6A1-4V plates were investigates in the 10^6 y 10^7 cycles range using changes in the resonance frequency as the means to detect fatigue damage.

Miguel Angel Moreles and Salvador Botello [57], published a paper developing the calculus of Natural frequencies in Elastic Beams with Shear effect and Rotational Inertia effect under multiple configurations such as, cantilever beam, simply supported beam, etc. using WPM (Wave Propagation Method) and compared their results with FEM (Finite Elements Method), showing the effectiveness of that method.

CHAPTER 3

NUMERICAL SIMULATION

In general a Timoshenko beam formulation is used to describe shear and rotational effects, neglected during Euler-Bernoulli beam modeling. The solution to the equation generated can become quite complex and can be either analytically or numerically solved depending upon the boundary conditions encountered. Because the vibration specimen designed will most likely have a varying geometric cross-section, Finite Element Analysis using ANSYS 11 was selected. Three elements: Beam, Shell and Solid were initially investigated for accuracy, computational efficiency and ease in modeling. The results using each element configuration were compared with a cantilevered Timoshenko beam [57]. The beam studied was constructed from aluminum with a length of 1555 cm, a width of 100 cm and thickness of 100 cm. The first three natural frequencies were calculated using elements of various dimensions. Results are shown in Table 3.1

Table 3.1: Results using beam, shell and solid elements for the first three natural frequencies of a Timoshenko beam

Type of element	1st mode (Hz)	2nd mode (Hz)	3rd mode (Hz)	Element Size
BEAM	3.5385	20.067	51.305	Length/40
SHELL	3.5333	20.712	49.02	Width/8
SOLID	3.53	20.186	47.61	Width/8

Even though, no significant difference can be found in using the various elements, the solid brick element was chosen because of its ease in programming varying geometry and its full 3-dimensional capabilities. In order to reduce the computational effort of this element, mesh size independency was investigated. Four mesh densities consisting of elements of one-half, one-quarter, one-eighth and one-sixteenth the beams width, were investigated in modeling the previously mentioned Timoshenko beam. The results of these tests are shown in Table 3.2. Elements corresponding to one-eighth and one-sixteenth beams widths predicted the same value for the first natural frequency and generated differences of less than six percent in the predicted second natural frequency. Thus by using an element of one-eighth, the beams width a minimal computational effort can be achieved.

Table 3.2: First three-natural frequencies obtained with various element widths

Resonance	Closed-Form Solution	Elements			
		Width/2	Width/4	Width/8	Width/16
1^{st}	3.55430	3.72 (4.45%)	3.61 (1.54%)	3.53 (0.69%)	3.53 (0.69%)
2^{nd}	19.01901	21.9 (13.1%)	21.5 (11.5%)	20.186 (5.7%)	20.01 (4.95%)
3^{rd}	42.307	51.43 17.7%)	48.5 (12.8%)	47.61 (11.5%)	46.97 (9.92%)

3.1 ANALYSIS OF FR-7140 FOAM

In order to develop the design methodology, initial work was performed using a polyurethane foam manufactured by “General Plastic Manufacturing Company”. This foam was selected because its availability, consistency in manufacturing and information of the material properties specified by the manufacturer. Table 3.3 shows the material properties that were given for the FR-7140 foam.

Table 3.3: Mechanical Properties of FR-7140 foam.

Property	**English**	**Metric**	**Test Method**
Density (pcf) (kg/m^3)	40	640	ASTM D-1623
Shear Modulus (G), (psi) (kPa)			ASTM C-273 Compression Shear
Rise Parallel to Specimen Width (Gxz)	26984	186057	
Rise Parallel to Specimen Thick (Gxy, Gyz)	24593	169570	
Flexural Modulus (E), (psi) (kPa)			ASTM D-790 Method 1-A
Rise Parallel to Beam Thick	163540	1127609	
Poisson's Ratio	~0.3	~0.3	Literature (Gibson and Ashby)

3.1.1 T.P.B. Analysis

Static and fatigue three point bending tests (TPB), were performed for various foam beams having dimensions of 16 cm in length, 3.81 cm in width and 1.9 cm in thickness. Testing was performed using the ASTM C393 standard [11]. Fatigue TPB was modeled using solid elements with vertical restrictions at the ends. Completely reversible (R = -1, ($\sigma_{min.} / \sigma_{max.}$)) center beam loading with a frequency corresponding to 0.75 Hz, was used. The Von MISSES stresses corresponding to the centerline were calculated and are shown in Figure 3.1

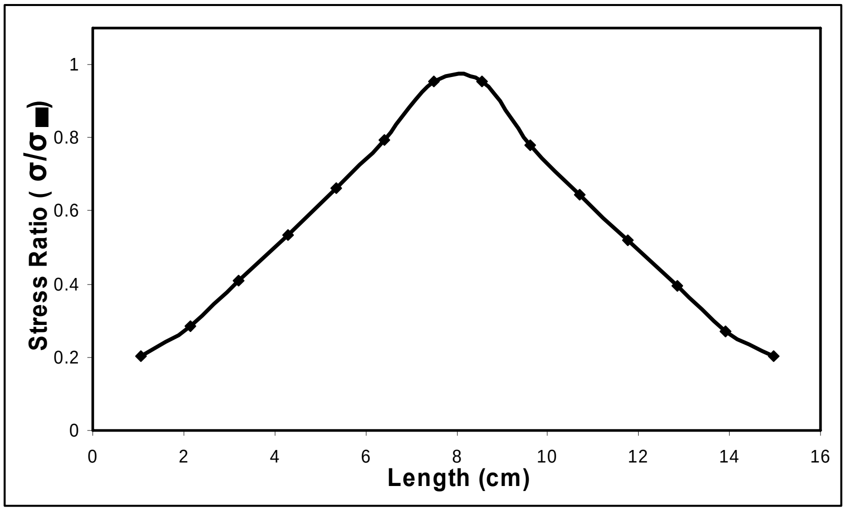

Figure 3.1 Stress pattern in TPB of FR-7140 foam

3.1.2 Vibration Analysis

In order to ensure that the FEA modeling predicted specimen behavior adequately, vibration testing was performed. A detailed description of the testing along with the experimental results is given in chapter five of this thesis. Six rectangular cantilever beam specimens were vibrated using a double cantilever beam configuration as depicted in Figure 3.2.

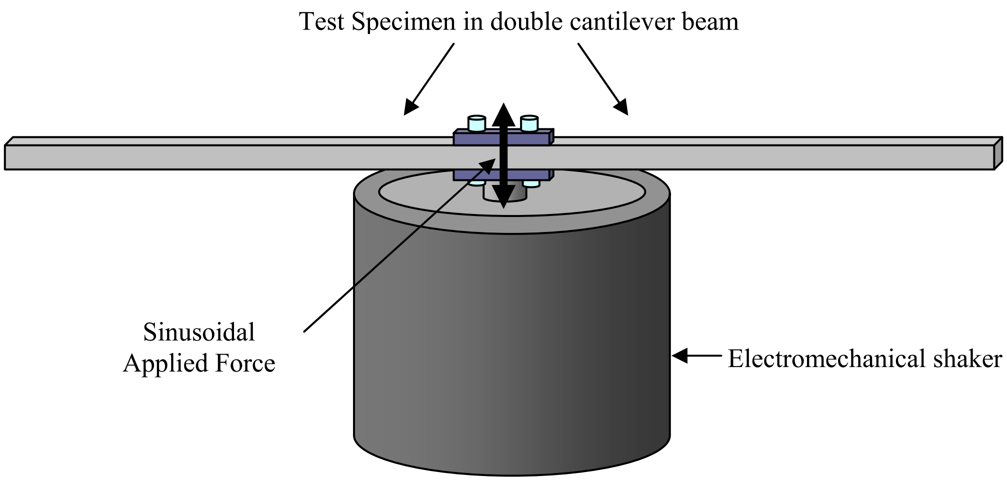

Figure 3.2: Experimental setup used in verifying FEA modeling.

Specimens consisted of a double length beam with equivalent cantilever dimensions of 39 cm in length, 4 cm width and 1.3 cm thickness. The frequency response function (FRF) containing the first three natural frequencies was determined by exciting the beam with random white noise. The FEA model used consisted of solid elements distributed along its length with a width corresponding to one eight the beam tested. By restricting the degrees of freedom at the cantilevered end appropriate boundary conditions were established. Performing computational modal analysis, values of 19.03, 109.45, and 321.40 Hz, were obtained. When compared to experimental results, these produced errors of 2.41, 2.77, and 8.84 percent. Table 3.4, shows the values and errors generated in process.

Table 3.4 First three natural frequencies from experiments and FEM

Natural Frequency	Experimental (FRF)	FEM (ANSYS) Solid (W/8)	Percent Error
1^{st}	19.5 Hz	19.03 Hz	2.41%
2^{nd}	106.5 Hz	109.45 Hz	2.77 %
3^{rd}	295.3 Hz	321.40 Hz	8.84%

Once an adequate model was established, a harmonic analysis occurring at each of the beam, first three transverse natural frequencies using the same forcing amplitude was performed. Here the Von Misses centerline stress pattern for a completely reversible loading was determined. The results of the three mode shapes are shown in Figure 3.3. It is clearly evident that the stress pattern generated at the first resonance is significantly greater than those corresponding to the second and third resonances. Based on this observation the first mode shape was selected as the starting point in the geometric specimen optimization procedure described next.

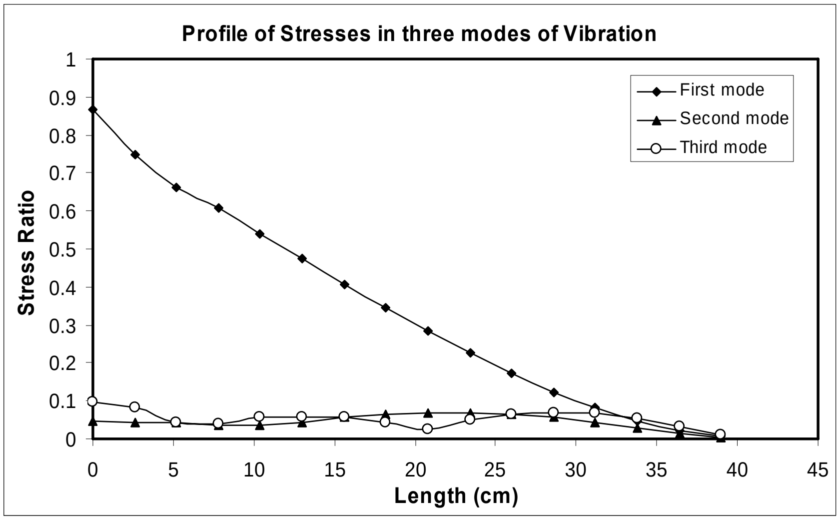

Figure 3.3: Comparison of the Von Misses centerline stress profile for the first three flexural transverse natural frequencies.

3.1.2.1 Geometric optimization

By examining Figure 3.3 it is evident that the highest stress occurs at the cantilever end during the first mode of vibration. In order to mimic three-point-bending in a given region, the stress profile must significantly change. This can be readily accomplished in two forms; the first is obtained by changing the loading pattern in other words, the boundary conditions or the geometry of the specimen, which is a more logical approach.

As a first step in this procedure, a parametric model of a cantilever beam with variable dimensioning is established. The model used is shown in Figure 3.4, here, H1, H2, H3 and H4 correspond to thickness values that can be varied located at a distance of zero, L1, L2 and L3 from the cantilevered end. The width of the beam is designated by W. Initial constraints based upon the shaker capabilities and available equipment set the maximum dimension of L3 to be 39 cm with a restriction of a first resonance less than 40 Hz.

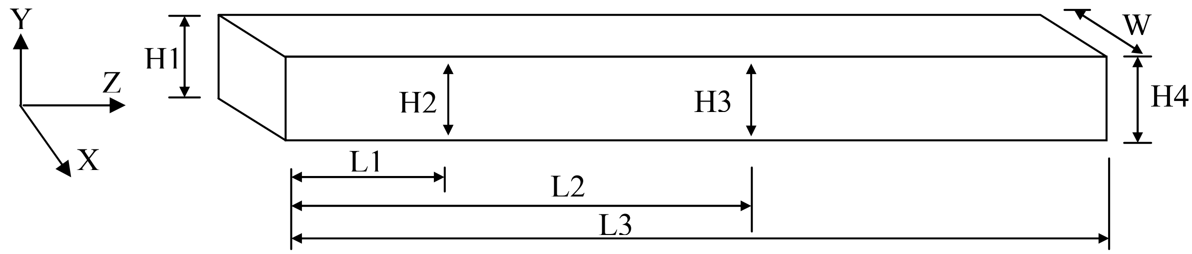

Figure 3.4: Parametric model used in geometric optimization

The vibration method used to produce the cantilevered boundary conditions consists of vibrating a beam at its midspan for all possible combinations of forced sinusoidal vibration. This produces an equivalent double-cantilevered configuration as shown in Figure 3.2. Figure 3.5 shows the free-body-diagram of the beam as examined from the static equilibrium position. By assuming an initial Euler-Bernoulli beam behavior and using elementary mechanics of materials (Gere) an equation, Equation: 3.1, can be established. This equation describes the stress at the cantilevered end of the beam.

$$\sigma = \frac{6 \cdot F \cdot L}{W \cdot H^2} \tag{3.1}$$

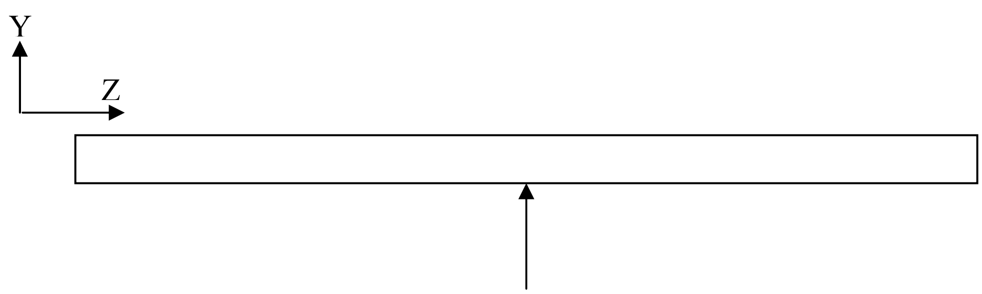

Figure 3.5: Free-body-diagram of the double cantilever beam used in the experiment.

Here F is the sinusoidal forcing function; L is the cantilevered beam length, W the beam's width and H the beam's height. By examing Equation 3.1 it is possible to notice that by either increasing the beam's height or width lowers the stress at the cantilevered end. In addition, small changes in height reduce the stress significantly more than chances in the width. This is due to the fact that the height appears with a greater power (H^2) in the denominator. Because of this, the height at locations H1, H2, H3 and H4 will be adjusted until the desired stress pattern is achieved.

The basic procedure consists of varying the H1, H2, H3, and H4 dimensions of an initial a rectangular specimen of uniform height of 1.27 cm. In order to reduce the stress at the cantilevered end, the thickness at location H1 is increased in ten percent increments of its initial value. After each change modal analysis is performed to determine the new stress pattern and ensure that the first resonance does not exceed the given constraint. This procedure is usually repeated several times until a decrease of twenty percent of the initial stress is obtained as seen by comparing Figures 3.6a and 3.6b. By decreasing the values of H2 and H3, the maximum stress occurring on the beam changes its location from the cantilever end. Again modal analysis is performed and values are examined to ensure that the changes are yielding desired output. It should be noted that during the process the values of H2 and H3 may be individually or simultaneously changed until the desired stress pattern is obtained. This process was repeated several times until the pattern shown in Figure 3.6c was obtained. Increasing the value of H4 furthers changes the stress pattern to resemble that found in TPB. Once again the interactive procedure of calculating the stress pattern and ensuring the first resonance is with limits was repeated. After several variations, the resulting pattern shown in Figure 3.6d was established. As seen in the figure the peak value generated a stress ratio of around 0.6 the ultimate stress found by TPB.

Varying the values of L1 and L2 can also alter the location and shape of the Von Misses stress curve. Here values were L1 and L2 were increased and decreased respectively to produce the Von Misses centerline curve shown in Figure 3.6e. A image of the final test specimen along with the mesh distribution used in the calculations is shown in Figure 3.7. A comparison of the Von Misses vibration centerline profile along with that obtained by TPB is shown in Figure 3.8. The process of alternating the values of H2, H3, H4, L1 and L2 can be continued to produce a better distribution similarity. However, the most critical region should be where the test specimen is designed to fatigue; the region was the highest stress ratio occurs as seen in Figure 3.8.

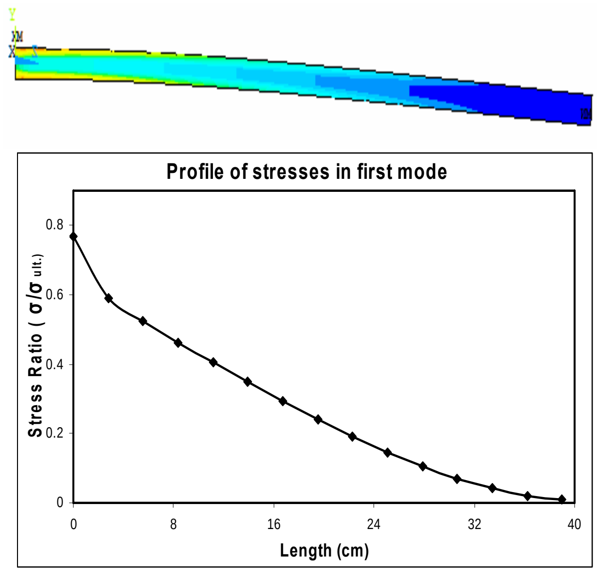

a) initial model

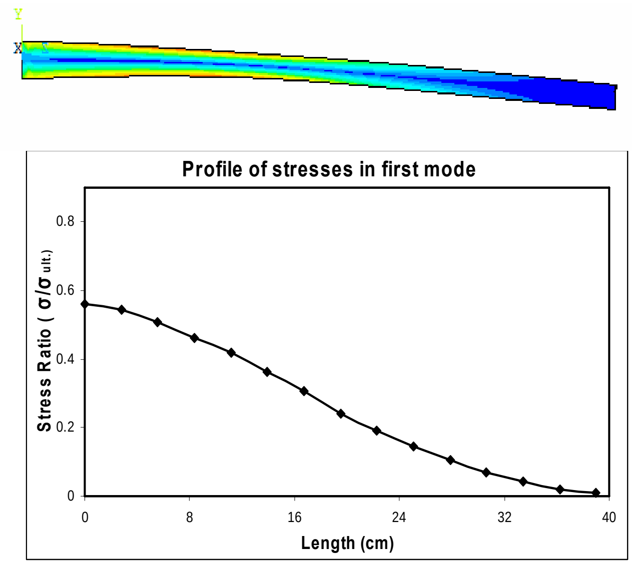

b) increasing H1

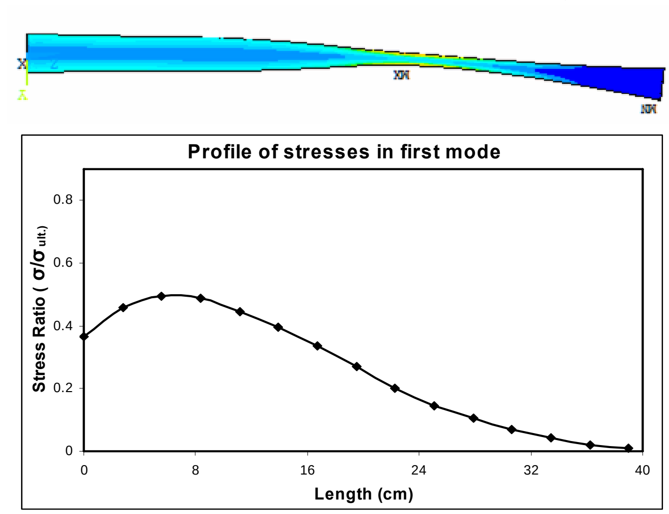

c) decreasing H2 and H3

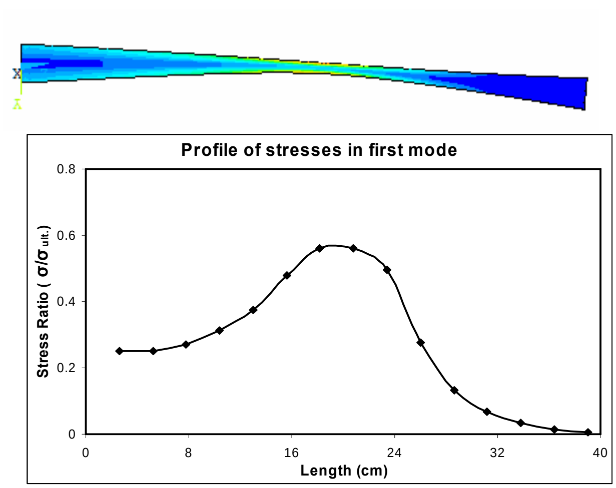

d) increasing H4

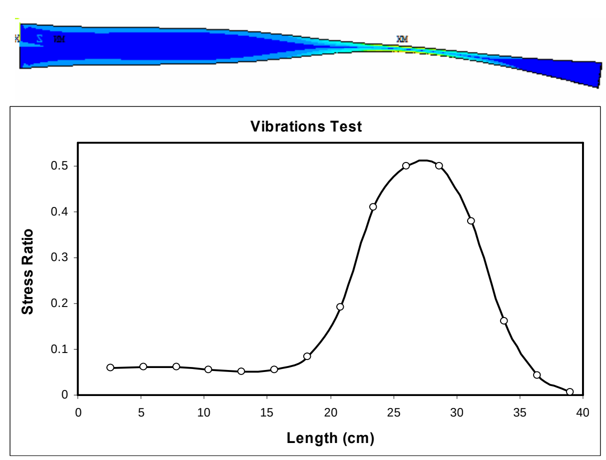

e) modifying L1 and L2

Figure 3.6: Geometric Optimization Process: a) initial model, b) increasing H1, c) decreasing H2 and H3, d) increasing H4, e) modifying L1 and L2

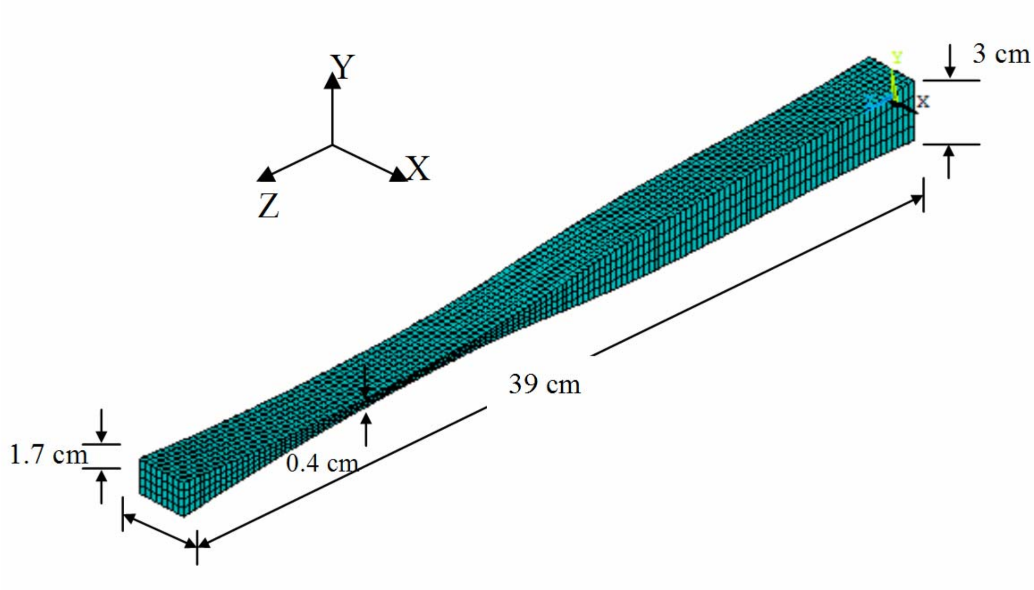

Figure 3.7: Optimized test FR-7140 foam test specimen with meshing used for analysis.

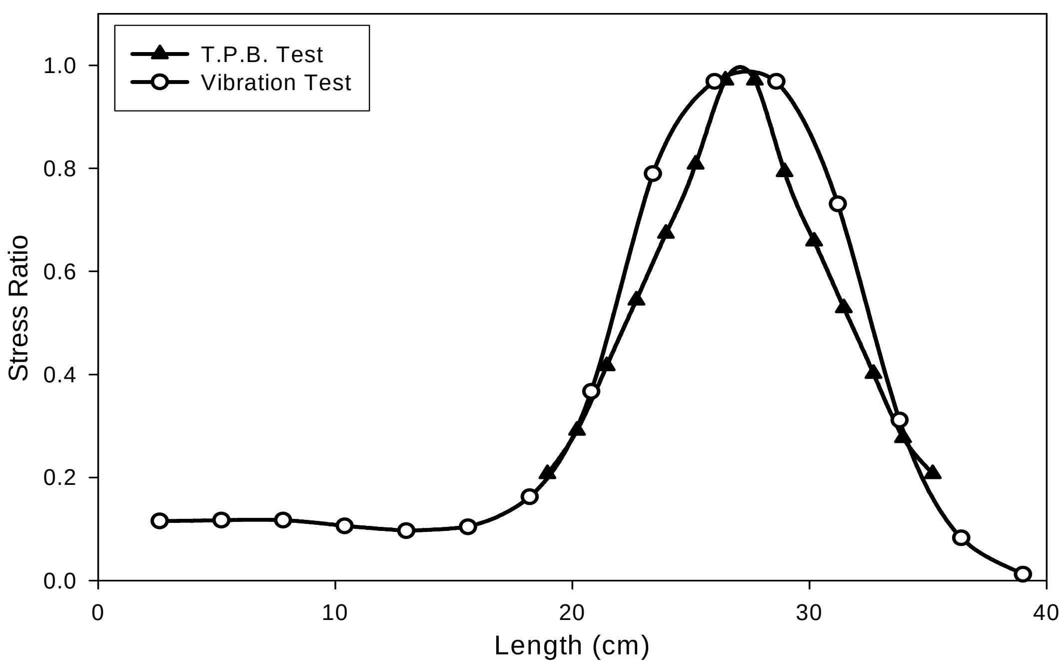

Figure 3.8: Comparison of the predicted Von Misses centerline stress profile from TPB specimens and vibration test specimens.

3.2 ANALYSIS OF SANDWICH COMPOSITES

Up to now, the methodology developed has been applied to an FR7140 foam beam. This section of the thesis will examine application to a sandwich composite. A sandwich beam will be constructed using facesheets with a 0-90 carbon-fiber weave bonded to a FR-7106 foam core with an epoxy resin. Unfortunately the exact values of the properties that characterize the behavior of the facesheets was unavailable, thus an optimization procedure to best estimate these values was developed. Once again, FEA using 3-D solid element modeling will be used. As before, the design procedure will yield a vibration specimen that mimics TPB in a desired region during a given resonance.

3.2.1 Fitting model parameters

The dimensions of the cantilever beam sandwich beam modeled consist of a length of 40 cm and a width of 3.81 cm. The core was FR-7106 foam and is 1.27 cm thick, 3.81 wide and 40 cm long. Figure 3.9 shows the sandwich beam with its corresponding dimensions.

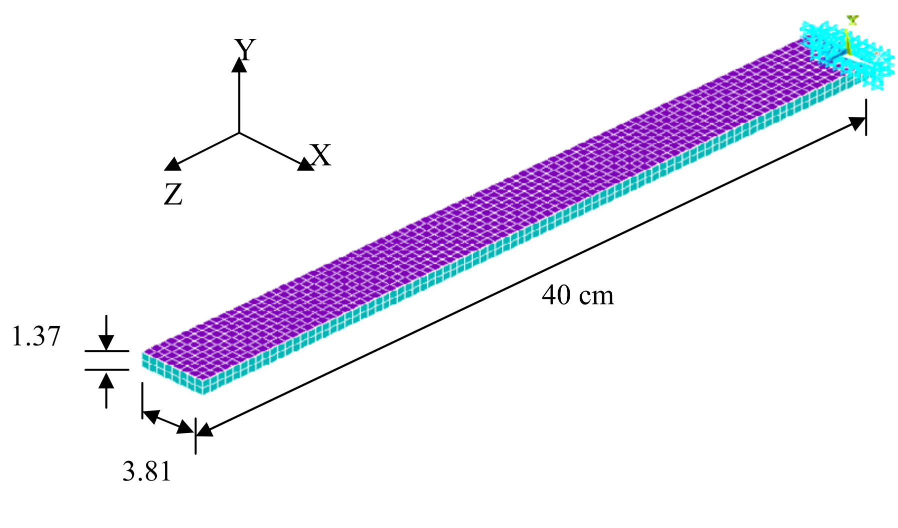

Figure 3.9: FE model used for the sandwich composite cantilever beam

The solid brick element used in modeling requires an input of eight material properties for both the facesheet and the core and are listed in Table 3.5. The core properties of the FR-7106 foam were obtained from the manufacturer and are given in Table 3.6.

Table 3.5: Linear composite element properties used in the 3-D solid element

Notation	Property
ρ	Mass density
E_x	Modulus of elasticity in X direction
E_y	Modulus of elasticity in Y direction
E_z	Modulus of elasticity in Z direction
G_x	Shear modulus of elasticity in X direction
G_y	Shear modulus of elasticity in Y direction
G_z	Shear modulus of elasticity in Z direction
υ	Poisson's Ratio

Table 3.6 Mechanical Properties of foam FR-7106 as supplied by the General Plastic Manufacturing Company.

Property	English	Metric	Test Method
Density (pcf) (kg/m^3)	6	96	ASTM D-1623
Shear Modulus (G), (psi) (kPa)			ASTM C-273 Compression Shear
Rise Parallel to Specimen Width (Gxz)	1251	8626	
Rise Parallel to Specimen Thick (Gxy, Gyz)	1304	8994	
Flexural Modulus (psi) (kPa) (E)			ASTM D-790 Method 1-A
Rise Parallel to Beam Thick	3119	21507	
Poisson's Ratio	~0.3	~0.3	Literature (Gibson and Ashby)

The facesheet properties are optimized with an objective function, *f*, that uses the predicted FEA natural frequencies, ω^n, and actual experimental frequencies, ω^e. The objective function is given in Equation 3.2 as:

$$objective\ \ function(f) = \left(\frac{\omega_1^e - \omega_1^n}{\omega_1^e}\right)^2 + \left(\frac{\omega_2^e - \omega_2^n}{\omega_2^e}\right)^2 + \left(\frac{\omega_3^e - \omega_3^n}{\omega_3^e}\right)^2 \qquad 3.2$$

In order to obtain values of $\omega_i^n (i = 1,2,3)$ eleven variables that must be evaluated. These values correspond to eight elastic properties in addition to three natural frequencies. The elastic properties of the FR-7140 were specified by the manufacturer and will remain constant during the optimization procedure. The actual values of the natural frequencies were obtained from experimental tests and correspond to values of 27.5, 245, and 665Hz.

The natural frequency of a structure is a function of its geometry, mass and elastic properties. In addition, the frequency can be sensitive to changes in some variables more than others. For this reason, a simple sensitivity analysis of the variables given in Table 3.5 was performed. Here FEA was used to predict the natural frequencies (with initial values obtained from literature [59]) and the objective function was evaluated. The results are shown in Figure 3.10. The properties corresponding to the variables E_x, E_y, G_{xz}, G_{yz} and υ (defined in Table 3.5) practically had no influence in varying the predicted natural frequencies. Thus maintain these values constant in the optimization procedure should not affect the results. This reduces the calculation to one using six variables $f(\rho, E_z, G_{z,} \omega_1^e, \omega_2^e, \omega_3^e)$.

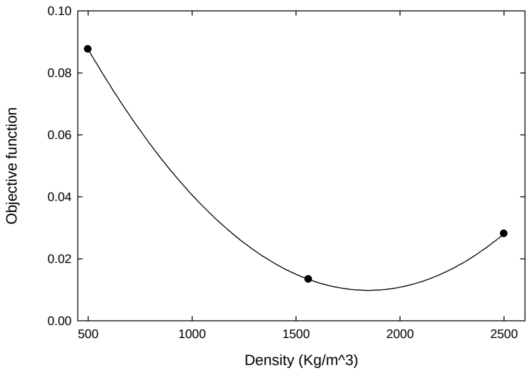

a) Mass density

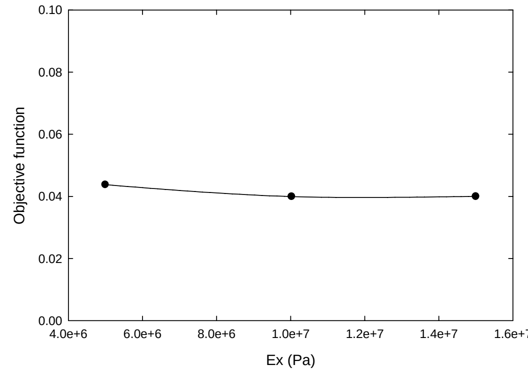

b) E_x modulus of elasticity

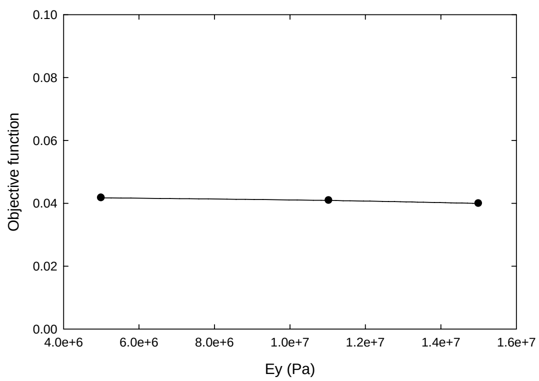

c) E_y modulus of elasticity

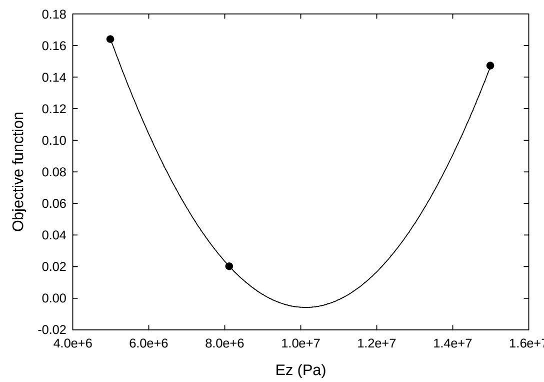

d) E_z modulus of elasticity

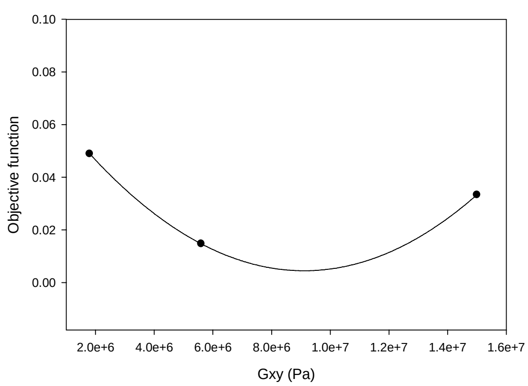

e) Shear G_{xy} modulus of elasticity

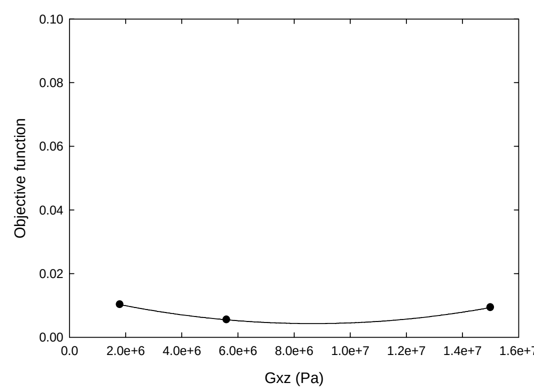

f) Shear G_{xz} modulus of elasticity

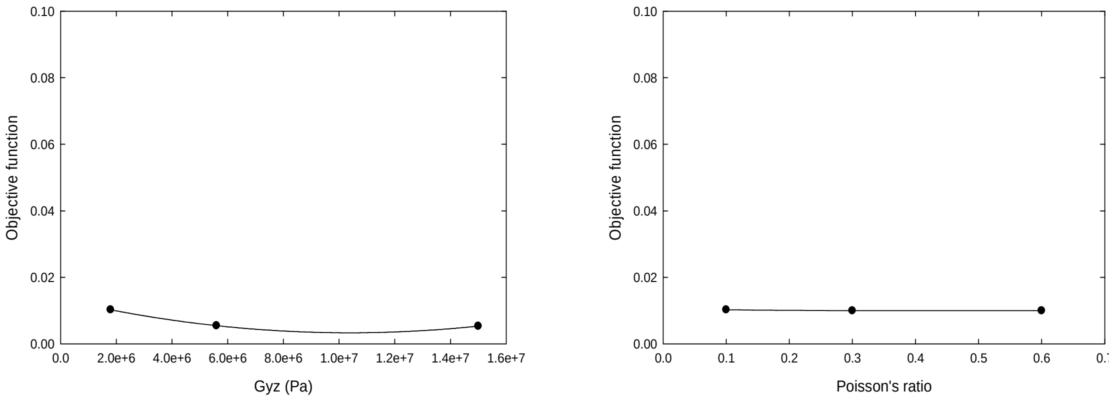

h) Shear G_{yz} modulus of elasticity g) Poisson’s ratio

Figure 3.10: Variation of the objective function subject to changes in the input parameters.

Since an explicit analytical expression for the natural frequencies is not available in terms of the elastic properties and only some discrete experimental values are it is necessary to apply an interpolation technique. The method chosen to optimize the reduced objective function was the quadratic interpolation method [Vanderplaats]. This procedure selects three initial values for the first variable ρ^1, ρ^2, ρ^3 and keeps the remaining variables E_z, G_{xy} fixed. The predicted FEA natural frequency values are then determined and the objective function is evaluated with those results. Afterwards, a second order polynomial $h_1(\rho)$ is used to approximate the objective function and a local minimum $(\rho^\bullet)$ is determined. The procedure is repeated for the second variable, E_x. Here the value of $\rho^\bullet$ is used for the variable ρ and three new initial values for the second variable (E_z^1, E_z^1, E_z^1) are selected. Again the natural frequency is evaluated and three new values of the objective function are obtained. A new second order polynomial $h_2(E_z)$ is defined and a local minimum for $E_z^\bullet$ is found. The procedure is repeated one more time for the last variable G_{xy} using the local minimum values of ρ* and E_x^* obtained previously. The predicted FEA natural frequency and objective function are evaluated using the three new estimates for ρ, E_x, and G_{xy}. This new value of the objective function is examined and if the criteria (a minimum is reached) is obtained, the procedure is terminated. However, if another set of iterations is required, the procedure described above is repeated. Figure 3.11 shows the results of the optimization method for the variables ρ and E_x and *Gxy*.

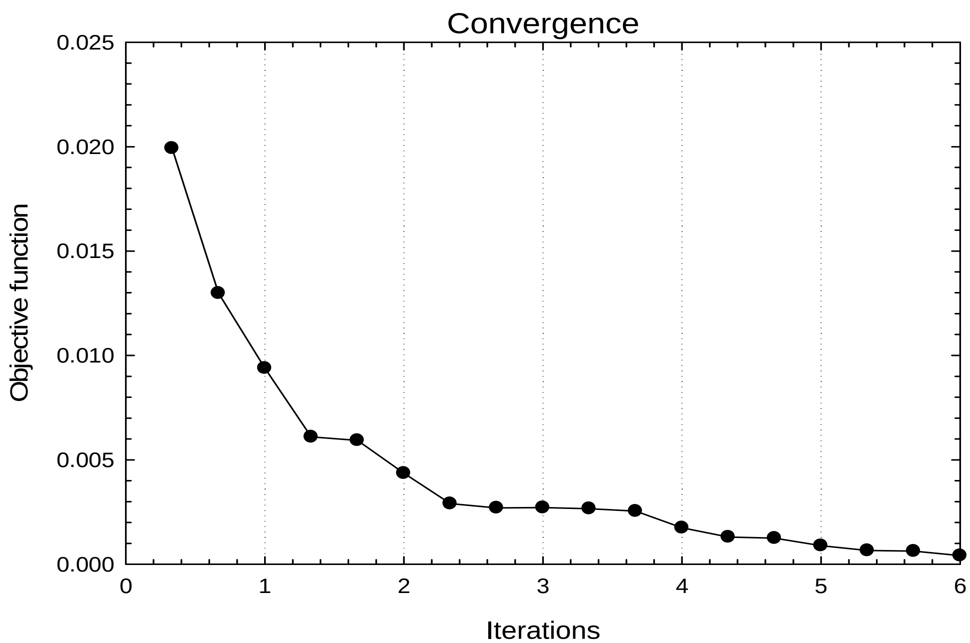

Figure 3.11: Objective function values during the optimization procedure.

With three complete iterations a satisfactory value of the objective function is obtained. However, in order to investigate the stability of the solution, six interactions are performed. Here the objective function yielded a value of 6.27 x $10^{-4.}$ By examining Figure 3.11 it is evident that the objective function converges to a local minimum. The final elastic properties obtained through this process are used in modeling and are given in Table 3.7.

Table 3.7: Optimized Elastic properties used in the FE model

Property	**Face sheet**	**Foam core**
Mass Density (kg/m^3)	1117	96
Longitudinal modulus of elasticity (MPa)	$40x10^3$	21.507
Transversal modulus of elasticity (MPa)	$40x10^3$	21.507
Longitudinal shear modulus of elasticity (MPa)	$10x10^3$	8.994
Transversal shear modulus of elasticity (kPa)	$10x10^3$	8.626
Poisson's Ratio	0.35	0.3

FEA modal analysis using the properties given in Table 3.7 for a cantilever beam configuration yielded a maximum error of 4% in predicting the first three transverse natural frequencies.

3.2.2 Three point bending analysis

Once the facesheet properties are established and verified, TPB modeling can be performed to determine the stress pattern to be mimicked. Here a sandwich beam having dimensions of 16 X 3.81 X 1.2cm using the aforementioned faceheet and a FR-7106 core was investigated. Modeling consisted of a completely reversible (R=-1, ($\sigma_{min.} / \sigma_{max.}$)) cyclical load exerted on the specimen using a sinusoidal excitation frequency of 0.75 Hz. The Von Misses centerline stress profile required for the vibration specimen design was determined and is shown in Figure 3.12.

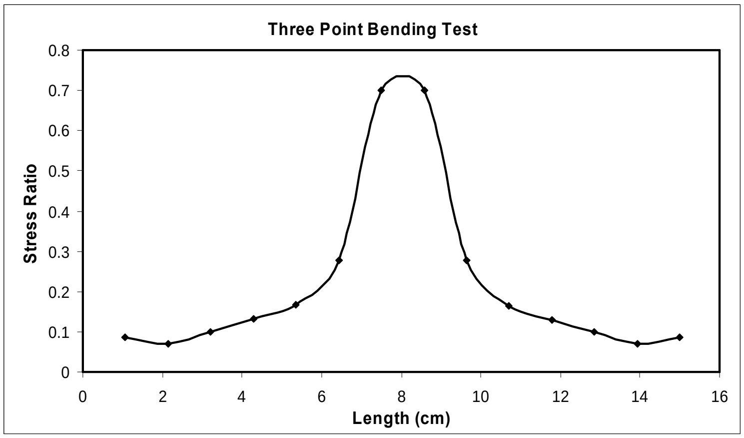

Figure 3.12: Von Misses centerline stress profile used in specimen design

3.2.3 Geometric optimization and Vibration analysis

As explained previously, the objective of this research is to design a vibration specimen capable of mimicking the stress profile found in TPB fatigue in a given region. In accordance with the section describing foam beam design, the cantilevered beam specimen will be vibrated at its first transverse resonance.

3.2.3.1 Geometrical optimization

From the foam beam analysis, it is evident that the highest stress levels occur at the cantilever end. Thus in order to establish a desired stress profile similar to Figure 3.12 geometric changes must be performed. This can easily be accomplished by either varying the facesheet or core thickness. However a better insight in the effects of changing these constituents can be obtained by considering the following hypothetical sandwich beam under a given bending moment *M* acting at its cross section (see Figure 3.13).

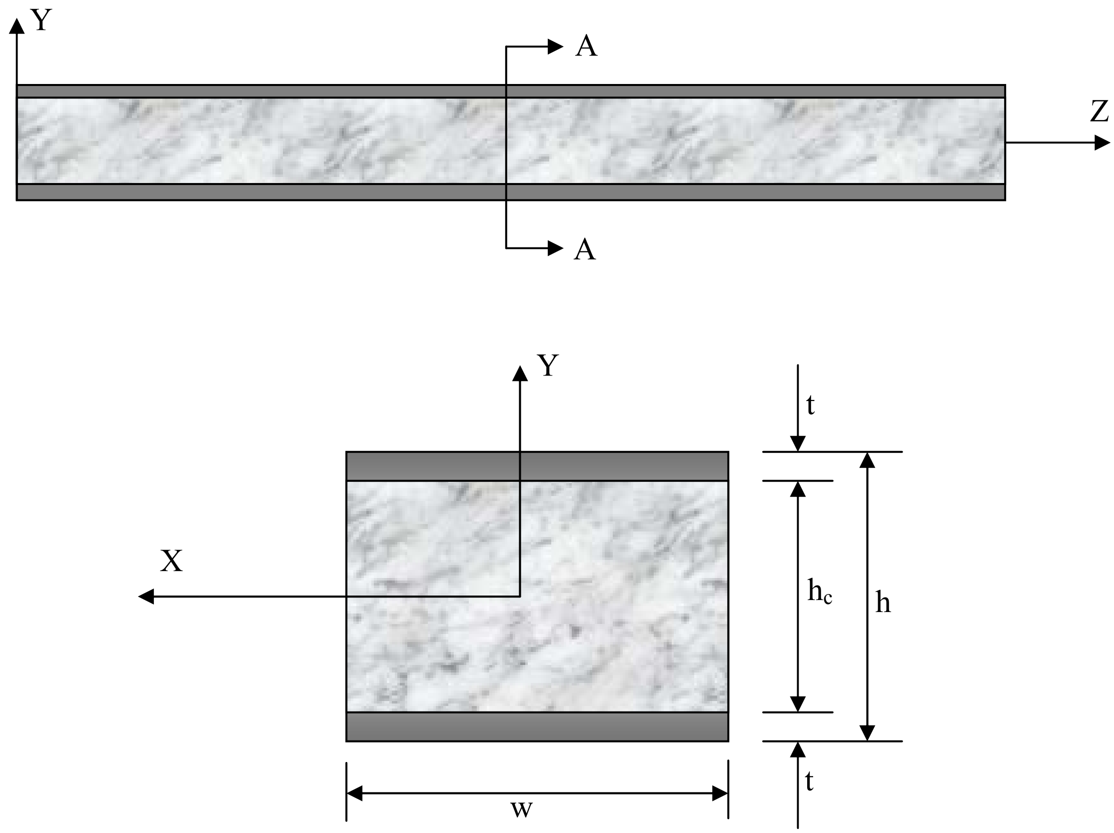

Figure 3.13: Cross section of sandwich beam under a given bending moment.

In the sandwich composite specimen to be designed, the modulus of elasticity of the face sheet is much greater than that of the core. When this occurs, the expression to determine the normal stresses in the facesheet can be given by $\sigma = \frac{My}{I}$. Here y is the distance from the neutral axis and I is the moment of inertia of the two facesheets evaluated with respect to the neutral axis. The maximum values of stress occur at the locations $y = \pm\frac{h}{2}$ and the moment of inertia of a face sheet may is given by $I_f = \frac{1}{12}wt^3 + wt\left(\frac{h}{2} - \frac{t}{2}\right)$. Assuming that the core is significantly thicker than the face sheet, for example h_c=$30t$, it is possible to get an idea of how changes in thickness of the constituents affect the stress. Consider the case when h_c=$30t$, increasing the facesheet thickness ten percent produces an 9.8 percent reduction of stress. However, increasing the core thickness ten percent yields a 16.95 reduction in stress. Thus by using the same procedure as described with the foam beam, the desired stress pattern mimicking TPB can be achieved by tailoring the core's thickness.

By establishing the parametric model shown in Figure 3.4, the vibration specimen may be designed. Due to the shaker and manufacturing equipment limitations, constraints corresponding to a resonance of less than 40 Hz along with a core length of no more than 39 cm will be established. Incrementing the value of H1 and then later reducing the values of H2 and H3 reduces and transfers the maximum stress (see Figures 3.14b and 3.14c. As in the case of the foam beam by increasing the value of H4, the stress pattern shown in Figure 3.14d begins to resemble that of the desired profile of Figure 3.12. Finally adjusting the values of L1 and L2 yields the stress pattern given in Figure 3.14e. It should be noted that after each modification a modal and harmonic FEA analysis must be performed in order to determine the new Von Misses centerline stress profile.

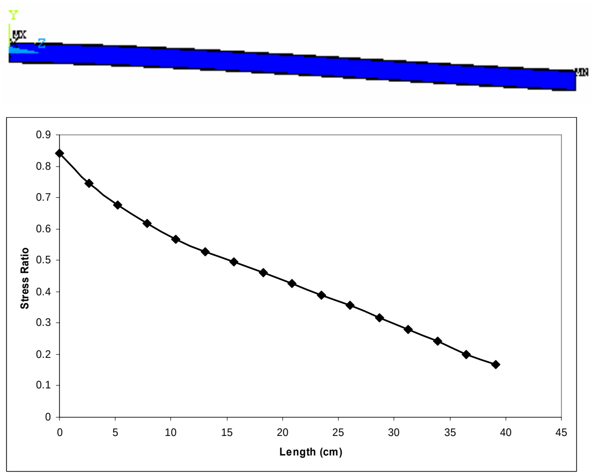

a) original initial model

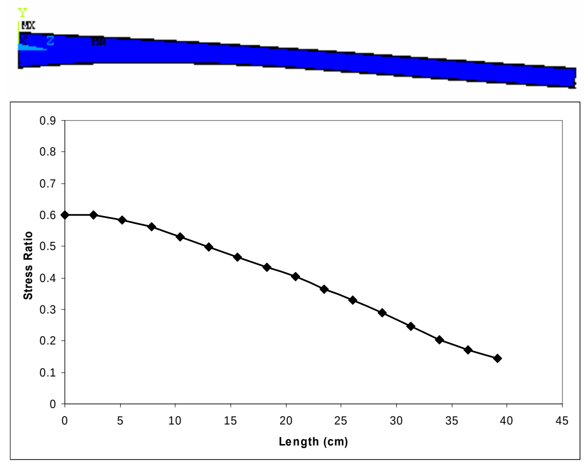

b) increasing H1

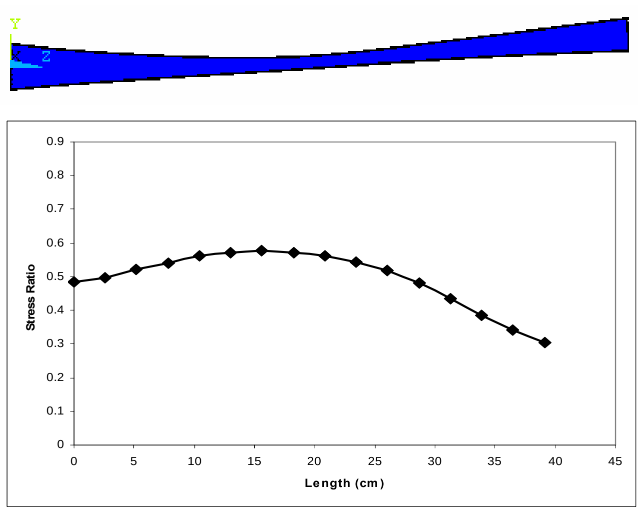

c) increasing H2 and H3

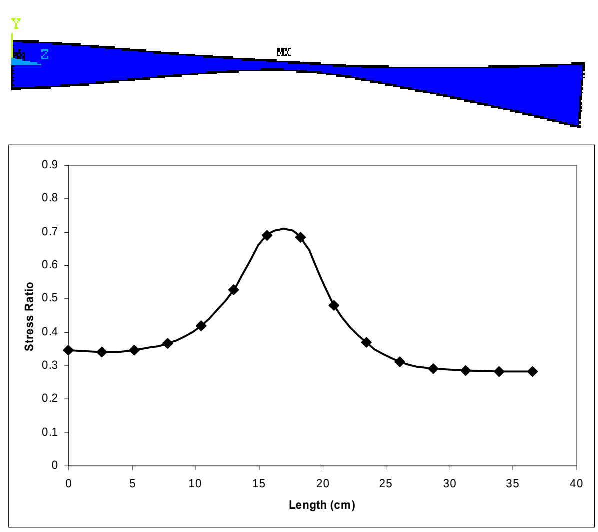

d) increasing H4

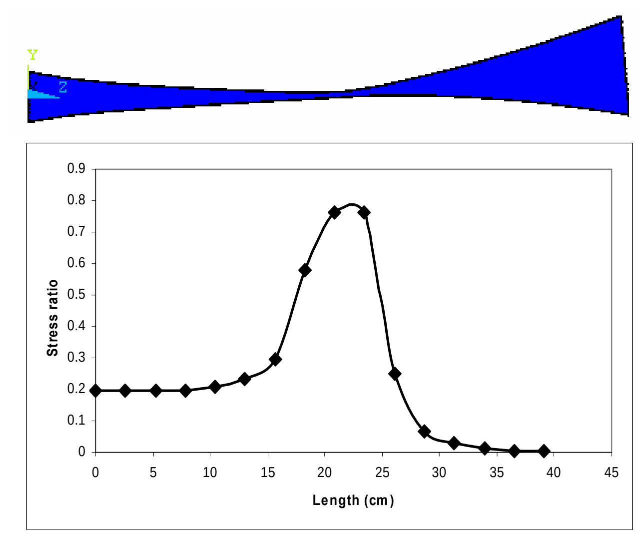

e) modifying L1 and L2

Figure 3.14: Geometric Optimization Process for the Sandwich composite a)initial model, b) increasing H1, c) decreasing H2 and H3, d) decreasing H4, e) modifying L1 and L2

The final optimized sandwich specimen is shown in Figure 3.15.

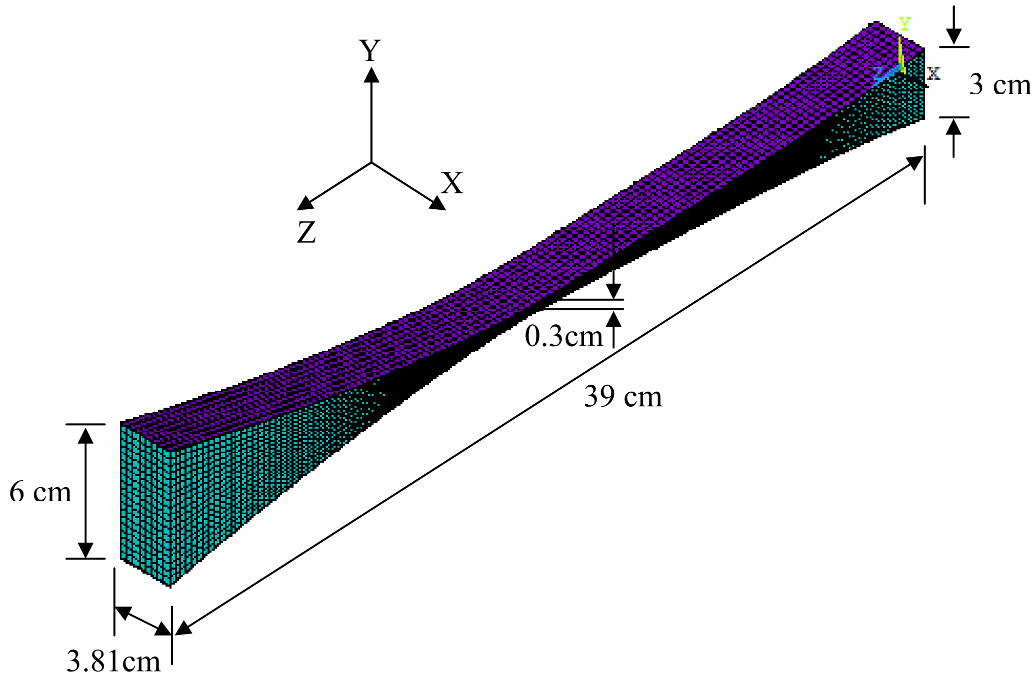

Figure 3.15: Optimized Sandwich Composite Specimen

Figure 3.16 compares the stress profile of the TPB specimen with that of the one designed using the aforementioned process. It is easy to observe that the profile in TPB is more acute than that of the optimized vibration specimen. A possible explanation of this is that the TPB specimen has a smaller length thus producing a greater curvature while under testing. Despite this difference in the profiles, the resultant specimen is still valid. This is because the greatest stress values occur in the area that is designed to fatigue during the vibration (see Figure 3.16). A finer approximation in the profiles could be obtained by further modification, however this would lead to a very thin region that would be unpractical to manufacture.

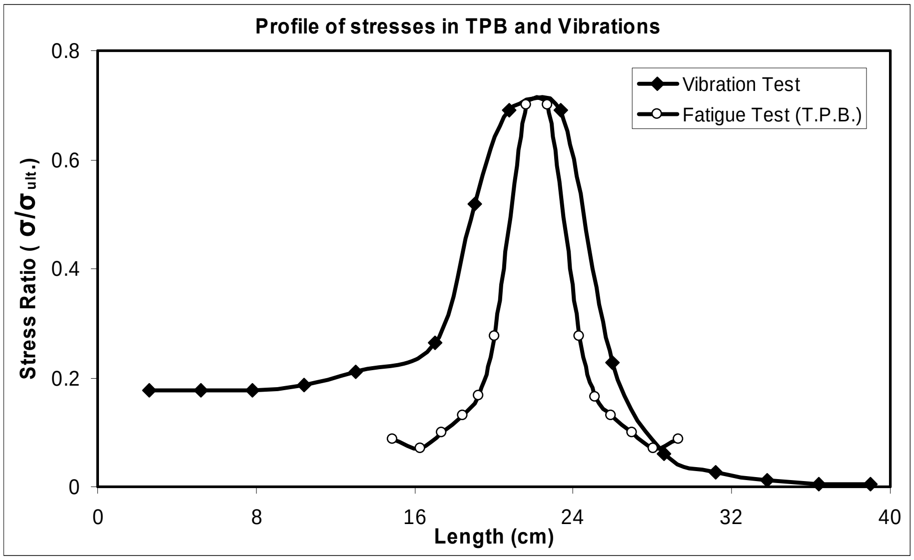

Figure 3.16: Comparison of the TPB and vibration specimen stress profiles

A flow chart of the optimization process used to design the vibration specimen is given in Figure 3.17.

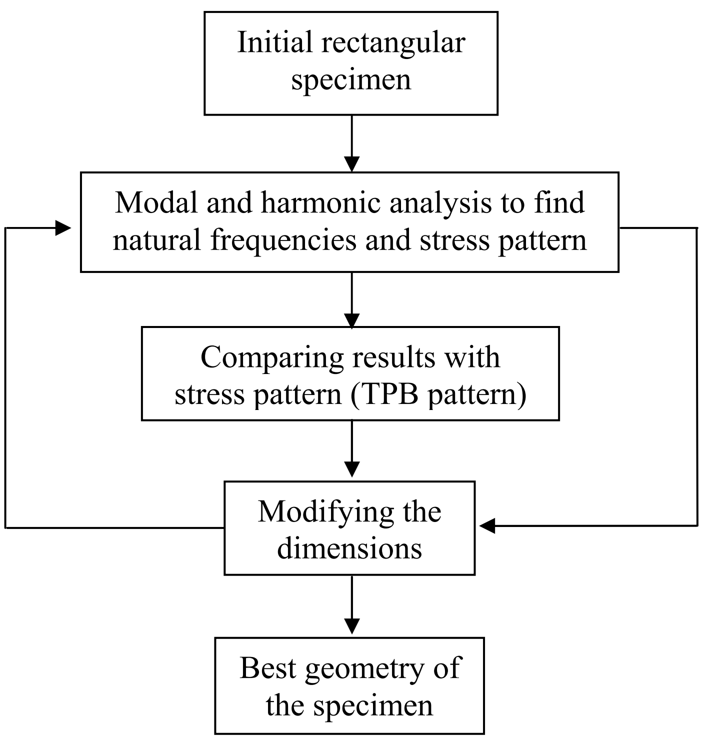

Figure 3.17: Sequence used in the vibration optimization process

Table 3.8 shows a comparison of the predicted FEA transverse natural frequencies and the obtained experimental frequencies. A maximum error 13.39 percent helps to demonstrate the effectiveness of this developed methodology.

Table 3.8: First three natural frequencies in FEA and experiments

Mode N^o	Optimized FE model (Hz)	Experimental specimen (Hz)	% Error
1	32.165	32.5	1.03
2	277.37	257.5	7.7165
3	581.34	671.25	13.39

Chapter 4

EXPERIMENTAL VALIDATION

In order to validate the specimen design methodology, experimental verification was performed. Experiments using TPB and a double cantilever configuration were used. Testing validated the procedure with polyurethane foam and sandwich composite beams designed with the methodology.

4.1 Experimental Equipment

An INSTRON MTS 810 servo-hydraulic machine was used for static and fatigue testing, shown in Figure 4.1. Static testing was performed using the ASTM C-393 standard. In addition fully reversible, (R=-1, $\sigma_{min.} / \sigma_{max.}$), TPB fatigue testing at room temperature was executed on both the polyurethane FR7140 foam and sandwich specimens. A 0.75 Hz sinusoidal loading frequency was used.

Figure 4.1: Material MTS 810 test system.

The total numbers cycles before catastrophic failure were recorded at various stress ratios. A Goodman Diagram S-N curve for both the foam and sandwich composite specimens was developed.

In order to maximize vibration testing, a constraint of a maximum sinusoidal excitation frequency of no greater than 40Hz was imposed. A VTS VG-150 electromagnetic shaker with a maximum capacity of 150 lbs, an operating frequency range of 0 to 4000 Hz and a 1-inch stroke was used for the vibration testing. Data analysis and excitation signal generation was done using a 6-channel DSPT SigLab Dynamic Signal Analysis (DSA) system. A Laser Doppler Vibrometer (LDV) was used to measure the beams transverse motion. Figure 4.2 depicts the experimental set up used.

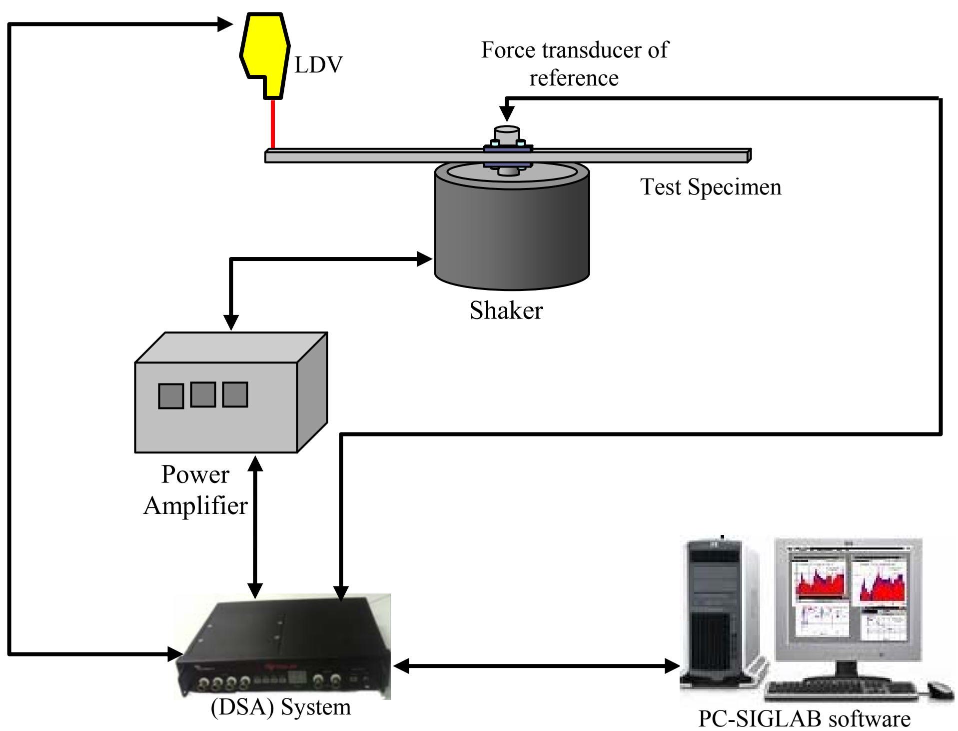

Figure 4.2: Schematic of experimental vibration setup.

4.2 FR-7140 Foam testing

4.2.1 T.P.B. Test

Before proceeding with the experimental TPB fatigue, static tests were conducted. Five specimens with dimensions of 16 X 3.81 X 1.27cm were tested in order to obtain the ultimate stress ($\sigma_{ult.}$). An average ultimate stress value of 25.2 Mpa with a standard deviation of 0.62MPa was obtained. Figure 4.3a and Figure 4.3b show the static test set up and a typical stress-strain diagram respectively.

Figure 4.3a: Static three-point bending

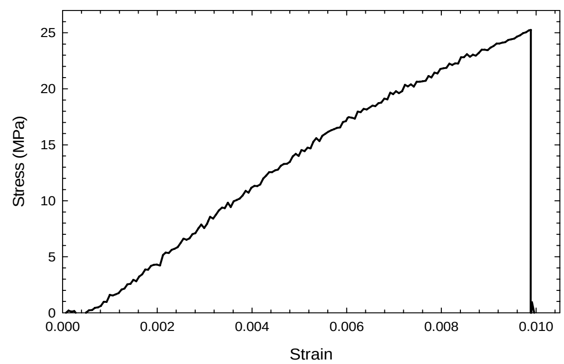

Figure 4.3b: Stress-strain diagram

In order to generate the FR-7140 foam beam fatigue curve, a total of sixteen specimens were tested. Four specimens were evaluated at four stress ratios, σ/σ_{ult}, corresponding to 0.55, 0.49, 0.43, and 0.39. Figure 4.4 shows a T.P.B. cyclic fatigue test being performed on a specimen.

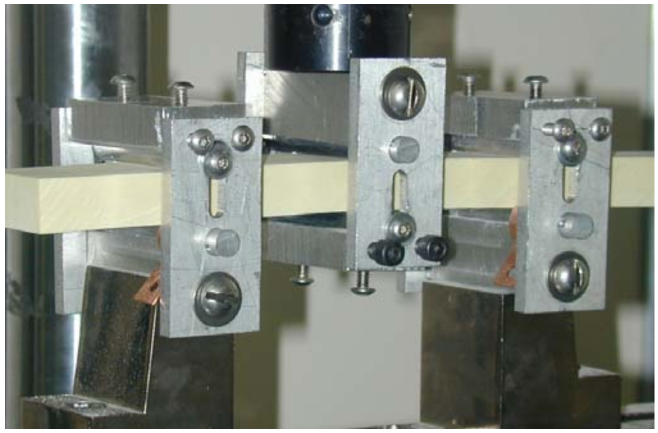

Figure 4.4: FR7140 foam beam under cyclic TPB fatigue testing**.**

4.2.1.1 TPB results

Specimens were fatigued at each stress level until catastrophic failure occurred. Table 4.1 gives the experimental data corresponding to frequency of loading, applied force, average number of cycles to failure and the average centerline displacement.

Table 4.1: Experimental results from T.P.B. test

Stress Ratio	Experimental Frequency (Hz)	Average cycles to failure	Applied Force (N)	Average measured displacement (mm)
0.55	0.75	2921	685	2.3
0.49	0.75	8091	630	1.75
0.43	0.75	18784	540	1.45
0.39	0.75	53359	490	1.25

The corresponding S-N diagram for this data is shown in Figure 4.5. Because the data seems to exhibit exponential behavior, the data was graphed using a semi-log scale as shown in Figure 4.6

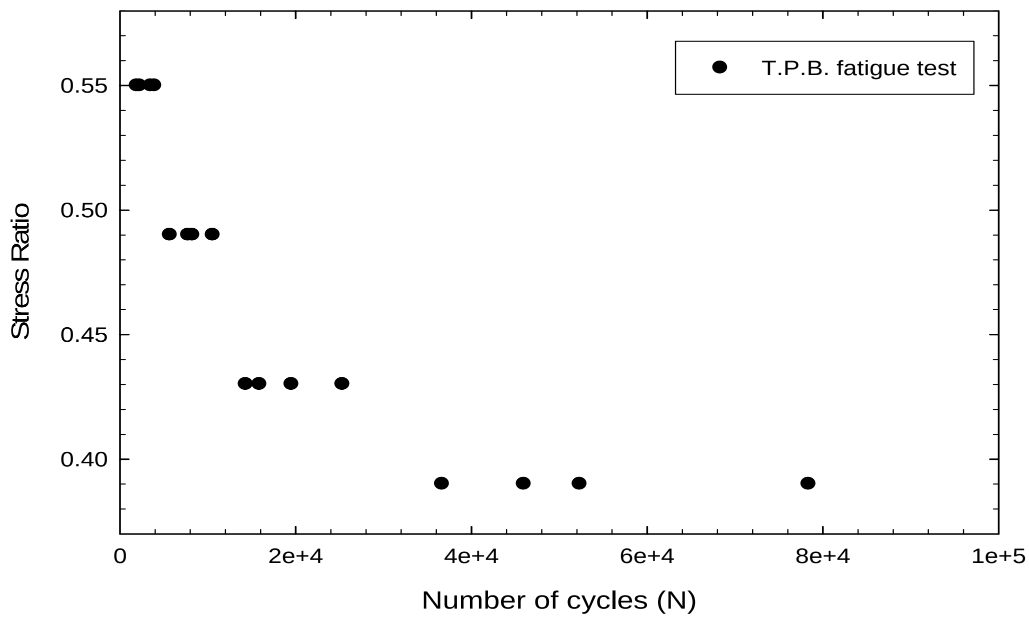

Figure 4.5: S-N plot of TPB fatigue data

Assuming an exponential relationship as suggested by several authors, [18, and 56] and deriving the least squares approximation constants of a best-fit line, Figure 4.6, the graph shown in Figure 4.7 was obtained.

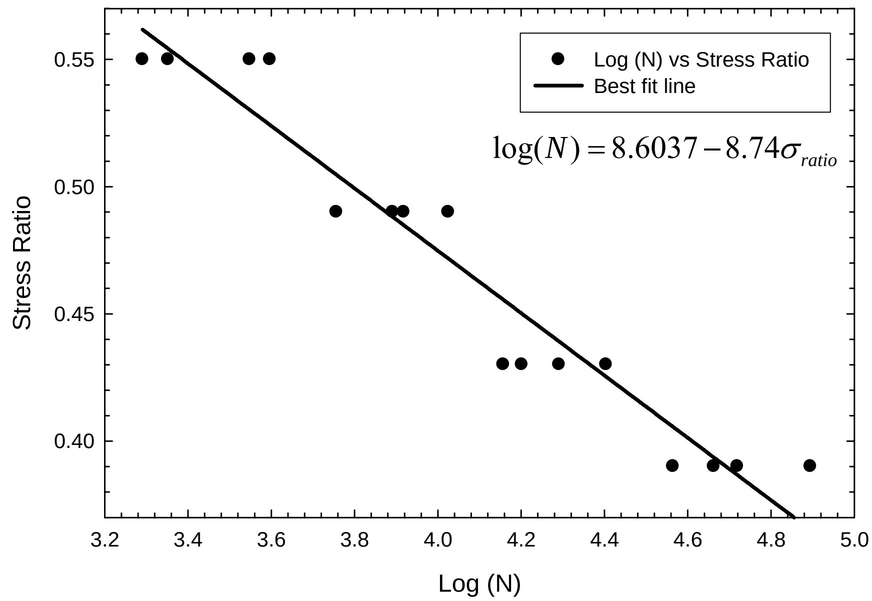

Figure 4.6: Semi-long scale representation of TPB data. .

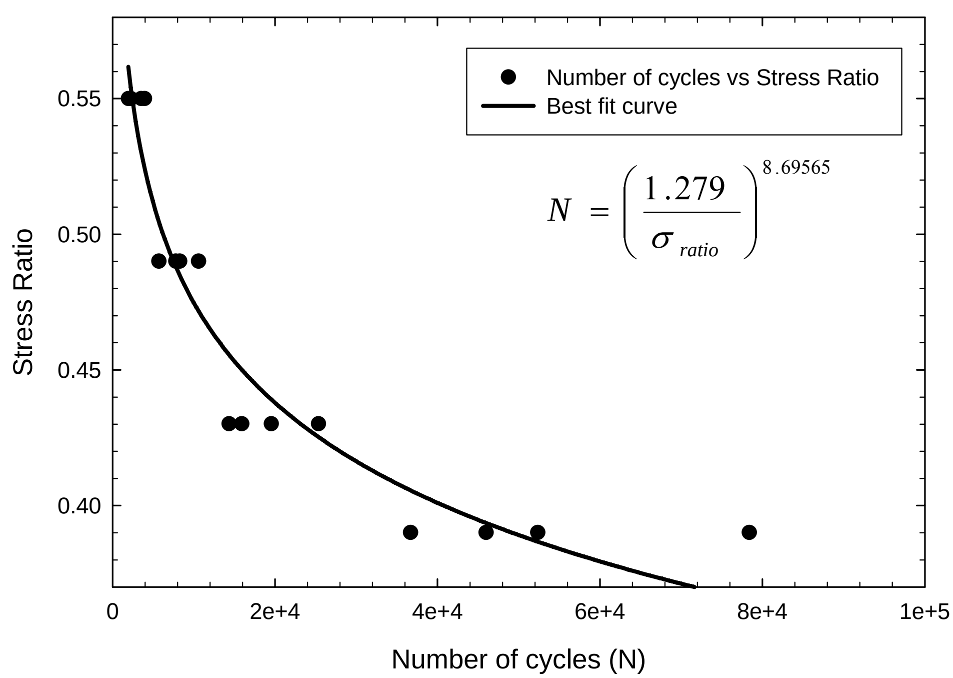

Figure 4.7: Exponential curve approximating lifetime behavior in TPB.

By examining Figure 4.6 and Figure 4.7, it is possible to notice that less data scatter occurs at higher stress ratios and at lower values an increased dispersion is observed.

4.2.2 Vibration Test

In order to validate the FEA modeling of the foam specimens, vibration testing was performed. Here the first two natural frequencies of each specimen were determined using a random noise excitation. Figure 4.8 shows a typical FRF (Frequency Response Function) plot.

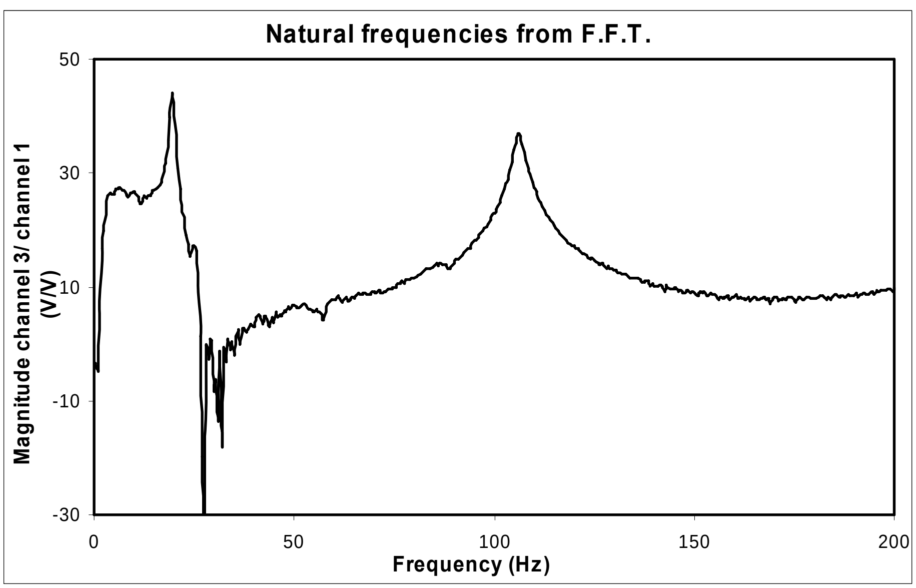

Figure 4.8: Typical FRF plot, from Modal Test

Once modeling was verified and the specimen was designed, manufacturing was performed. The specimen manufacturing process can be divided into the following steps:

1. Specimen dimensions are obtained from the FEA modeling and geometric information is exported into a computer aided drafting package such as Auto-CAD.
2. From Auto-CAD the geometry is read using the CNC program package GIBSCAM. This program generates the code needed to control the milling machine used to cut the specimen from foam block.
3. Final manufacture was performed on a CINCINNATI Milacron ARROW 500.

Figure 4.9 and Figure 4.10 show the FEA model of the specimen along with the final manufactured specimen respectively.

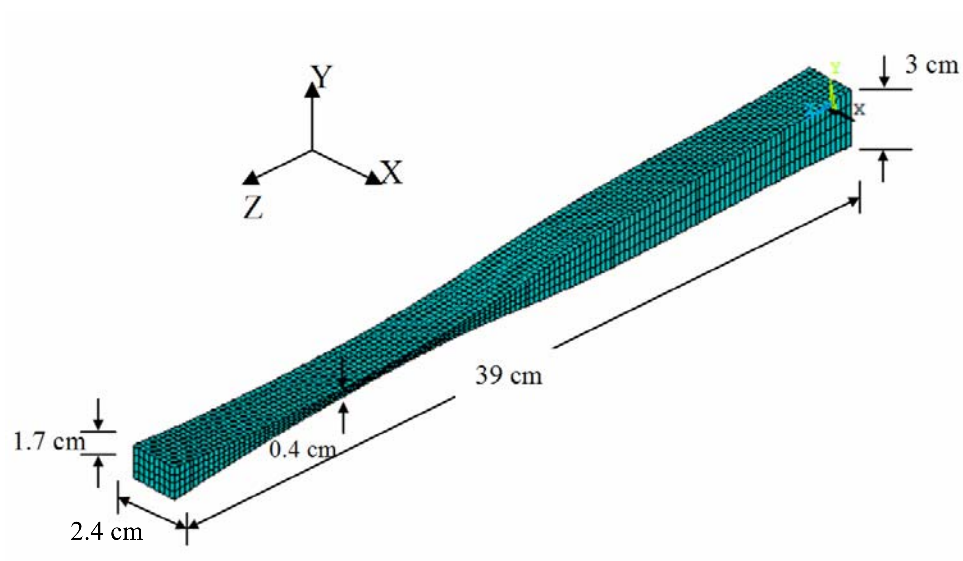

Figure 4.9: FEA model of the final specimen design

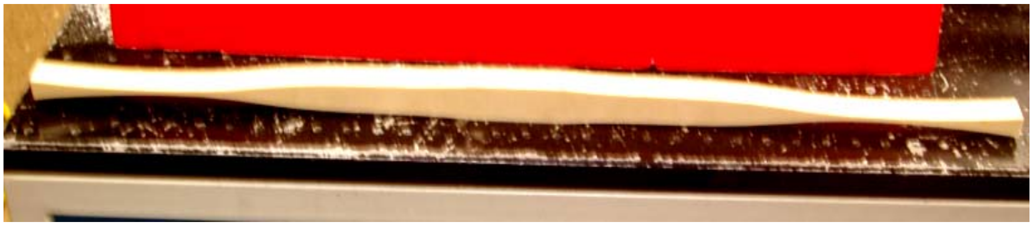

Figure 4.10: Actual manufactured specimen.

The specimens were mounted using the double cantilever configuration shown in Figure 4.11. Fatigue testing using a harmonic signal was performed. Here a force transducer measured the input force and amplification adjustment was implemented until the desired stress ratio was obtained. The lifetime of each specimen was determined with the input frequency and time required to failure. By evaluating specimens under different stress ratios the data required to generate a S-N curve for the FR-7140 foam specimens was obtained. Vibration testing was performed at room temperature. As with TPB testing 16 specimens were vibrated (four specimens for each stress ratio). The values of stress ratios (0.55, 0.49, 0.43, and 0.39) were similar to those used in TPB. Figure 4.12 show a specimen in resonance vibration.

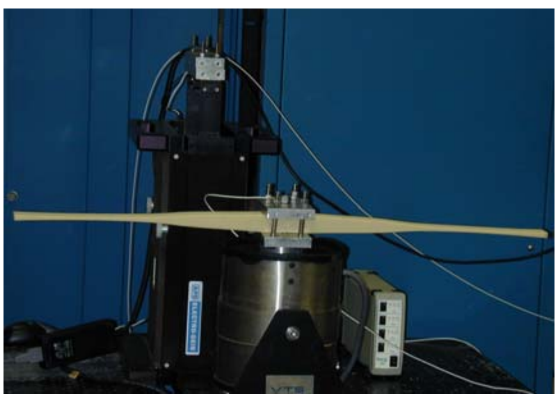

Figure 4.11: Experimental test setup

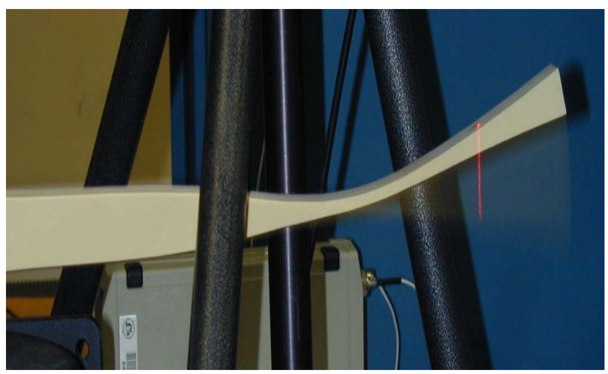

Figure 4.12: Specimen vibrating.

4.2.2.1 Experimental Vibration Results

Vibration fatigue analysis was performed until catastrophic failure occurred. Table 4.2 shows results obtained from testing along with the predicted values from the FEA modeling used to design the specimen.

Table 4.2: Experimental results from vibration test.

Stress Ratio	Experimental Result (Hz)	Predicted Frequency (Hz)	Average cycles to failure	Applied Force (N)	Average measured displacement (cm)	Predicted displacement (cm)
0.55	18.9375	19.295	4971	32.1	4.15	4.08
0.49	18.9375	19.295	10937	27.4	3.825	3.79
0.43	19.125	19.295	26643	21.94	3.39	3.405
0.39	19	19.295	78788	16.71	3	3.12

As with TPB, vibration fatigue exhibited an exponential behavior, Figure 4.13. By plotting data on a semi-log scale and obtaining a least square line approximation, Figure 4.14, an exponential curve similar to the one obtained TPB is generated, Figure 4.15. It is also interesting to note that the same type of scatter behavior found in TPB is also observed with the vibration technique.

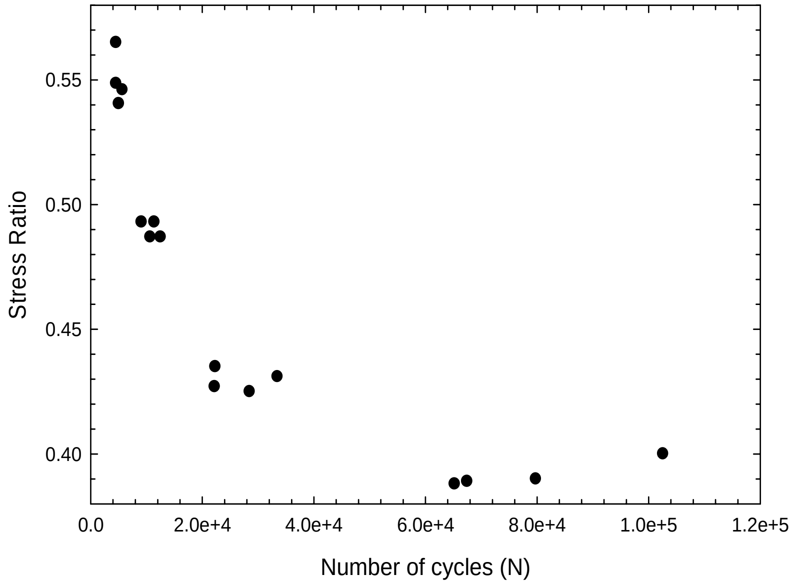

Figure 4.13: Plot lifetime data for FR7140 foam using vibration methodology developed

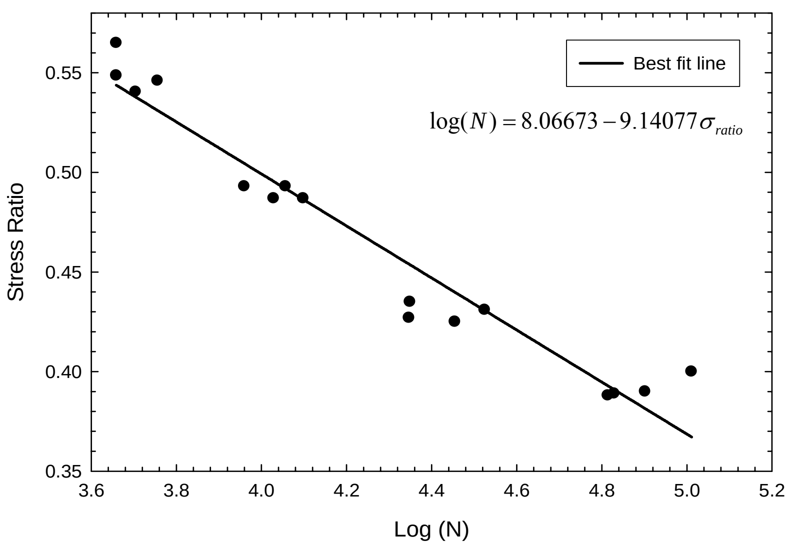

Figure 4.14: Semi-long scale representation of vibration fatigue data

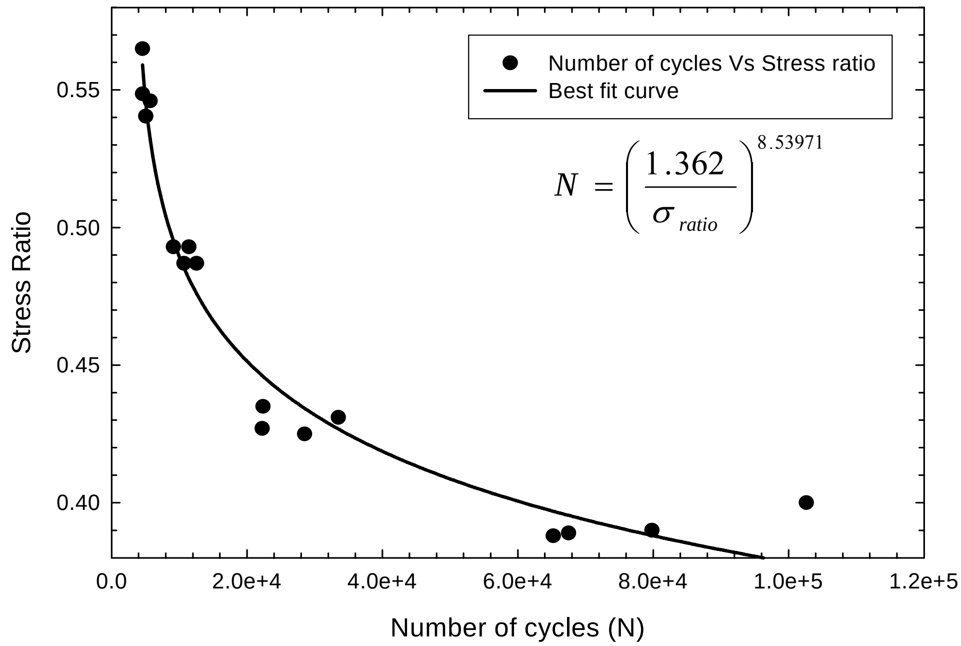

Figure 4.15: Exponential curve approximating lifetime behavior using vibration technique.

4.2.3 Thermal Analysis

Since temperature has been observed to reduce the lifetime of foams [21, 22] and in order to ensure that the vibration methodology did not generate excessive heat, several preliminary experiments conducted at room temperature, (15 °C) , were performed. The beam's temperature was measured at several locations using T type thermocouples with a precision of ± 0.1°C around the point of highest stress. Table 4.3 shows the results of average increase of temperature from the experimental fatigue test.

Table 4.3 Increment of temperature during fatigue test

Material	Number of specimens	First mode of Vibration average (Hz)	Increment of Temperature (°C)
Foam FR-7140	4	19.5	1.5 ± 0.6

Based on the data given in Table 4.4 it is possible to conclude that the increase in temperature is minimal. One possible explanation can be related to the frequency at which the tests are conducted. During vibration, the beam most likely undergoes a forced convective cooling that prevents extensive heat accumulation during the test.

4.3 Sandwich Composite Specimens

4.3.1 Manufacture and drying time

The composites specimens made consisted of a carbon-fiber facesheet (5.2 oz 0/90 weave) bonded to a FR-7106 foam core using an epoxy resin manufactured with the VARTM method. In order to ensure that the correct drying time had occurred, specimens were tested with static loading every day after the initial manufacture (see Figure 4.16). Twenty days after manufacturing repeatable ultimate stresses was obtained. Figure 4.17 shows the ultimate load as function of curing time. Result of these tests revealed that specimens dried one week or less presented wrinkling and indentation failures, but those with more than 12 days of drying always presented core shear failure as shown in Figure 4.18.

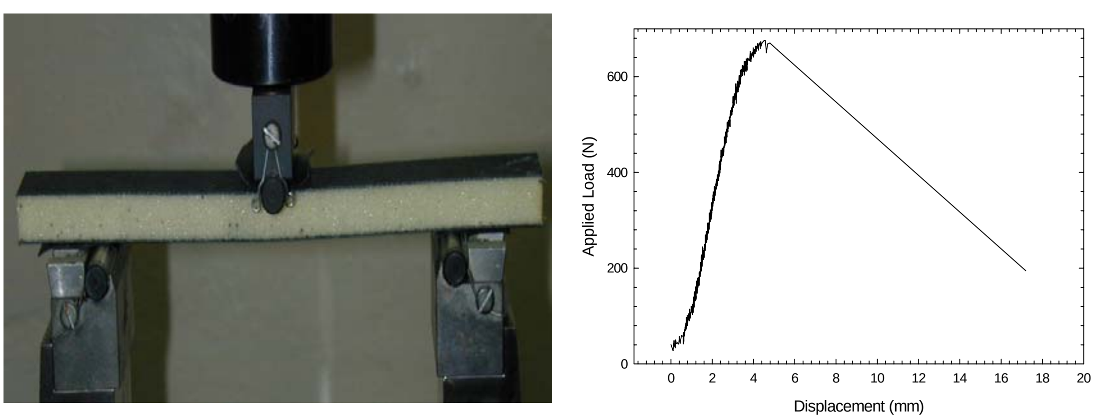

Figure 4.16: Static test setup for curing time evaluation with typical output

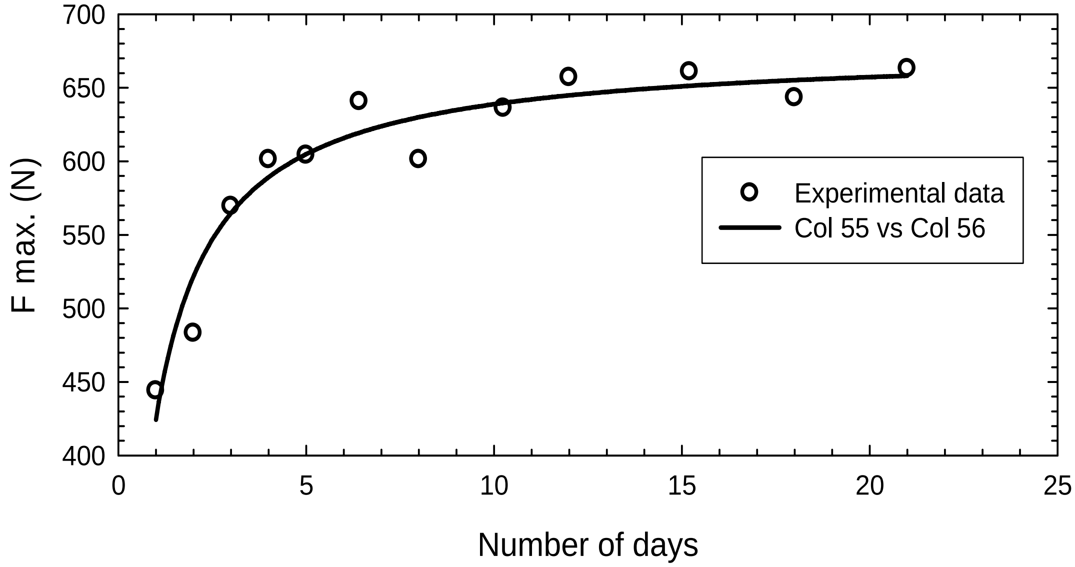

Figure 4.17: Curing time as a time after manufacture

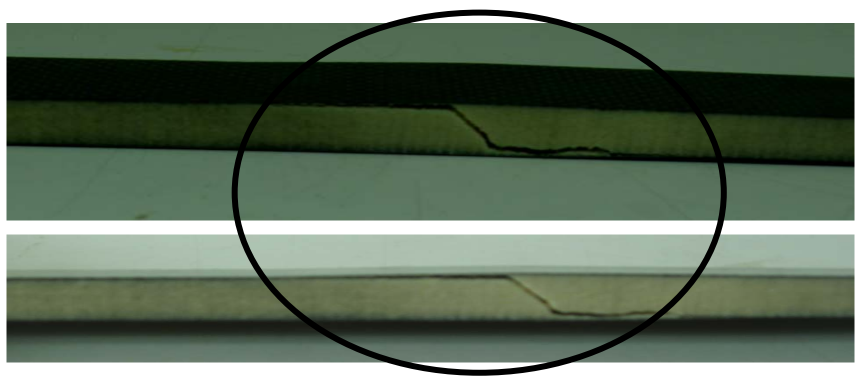

Figure 4.18: Shear core delamination failure after 20 days of drying

4.3.1.1 Experimental TPB results

As with the foam specimens, TPB fatigue tests were performed. Five specimens were tested at each of the four stress ratios (0.77, 0.70, 0.62, and 0.55). Shear core failure with facesheet debonding always occurred in very failure. Table 4.4 shows the results for these tests.

Table 4.4: Experimental results from T.P.B. test

Stress Ratio	Experimental Frequency (Hz)	Average cycles to failure	Applied Force (N)	Average measured displacement (mm)
0.77	0.75	4507	510	3.27
0.70	0.75	14726	460	2.69
0.62	0.75	66741	410	2.28
0.55	0.75	166742	360	2.112

Cycles to failure at each of the four stress ratios was plotted to generate the S-N curve for the sandwich composite vibration specimens (see Figure 4.19). Similar to the foam results exponential behavior was noticed and a best-fit linear regression line was obtained by plotting the data in a semi-log manner as shown in Figure 4.20. Once the exponential behavior was verified, the resultant exponential curve was determined and graphed, Figure 4.21. As with the previous foam analysis the specimens showed an increase in scatter with decreasing stress ratio.

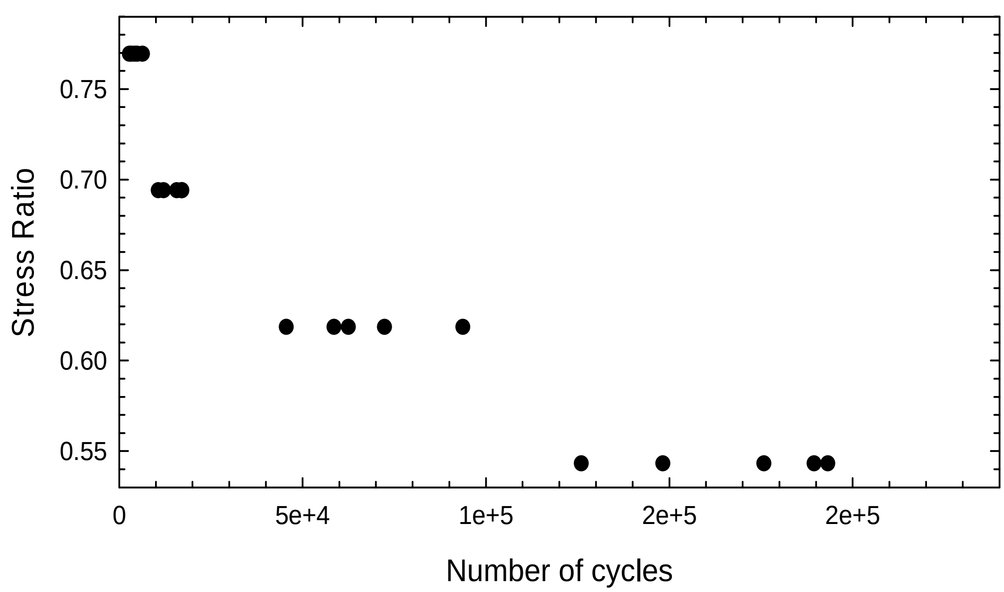

Figure 4.19: S-N plot of sandwich composite specimens tested in TPB.

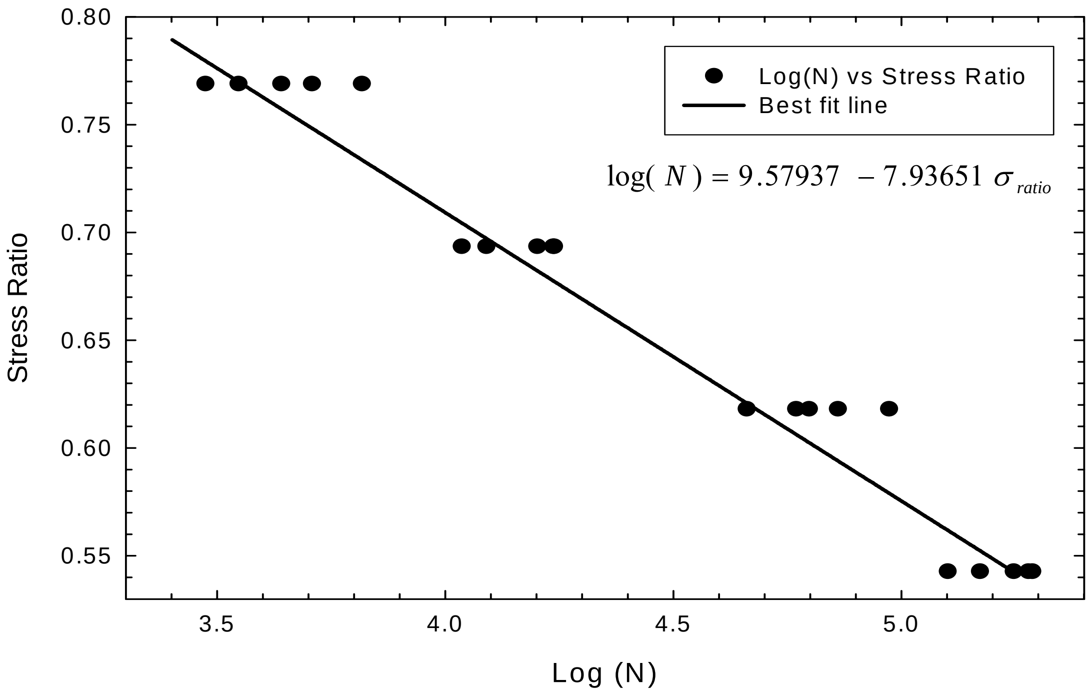

Figure 4.20: Confirmation of exponential behavior by plotting S-N data in a semi-log format.

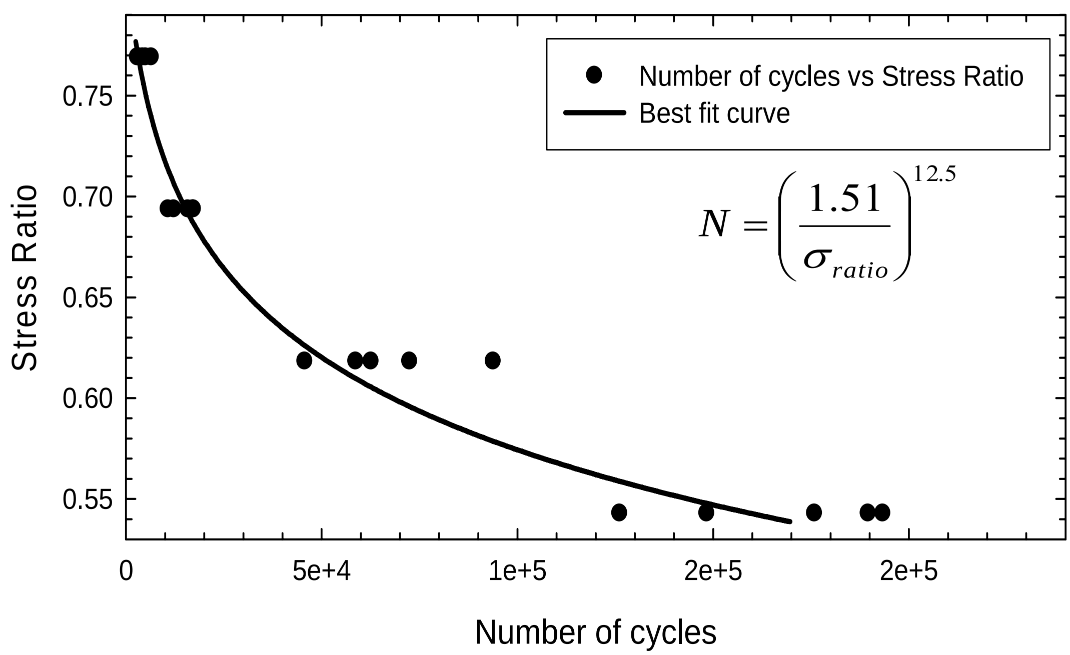

Figure 4.21: Best fit curve of exponential behavior observed in sandwich composite S-N data.

4.3.2 Vibration testing

Vibration specimens were designed with core modification. The design sequence for the sandwich foam core geometry uses the exact procedure for the foam specimens. Once the foam core was manufactured carbon-fiber face sheets were laminated with the VARTM process. A period of 20 drying days was allowed to ensure proper curing of the epoxy resin used. Figure 4.22 shows the final sandwich specimen designed for vibration fatigue testing.

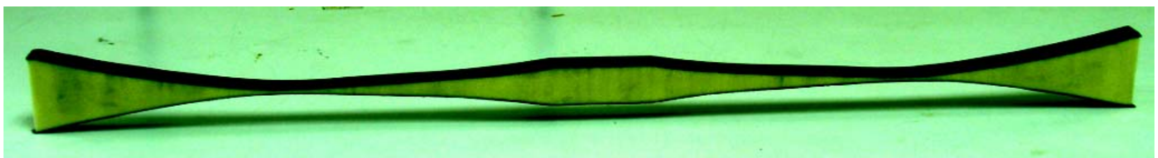

Figure 4.22: Final sandwich specimens design used in fatigue vibration.

As with TPB five specimens were evaluated at each of the four stress ratios used (0.77, 0.70, 0.62, and 0.55). Specimens were mounted using a double cantilever technique as shown in Figure 4.23.

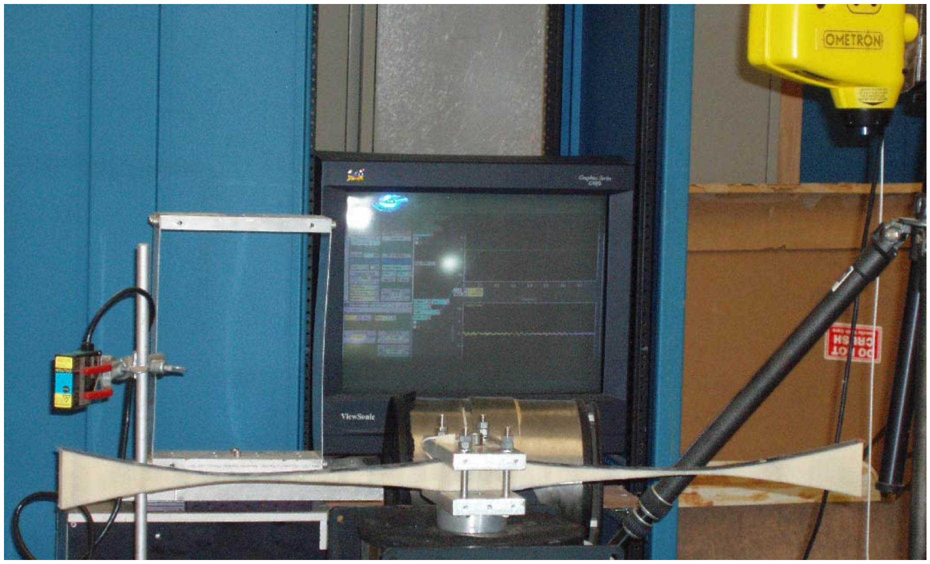

Figure 4.23: Composite specimen vibration using the double cantilever technique.

In this technique the fatigue limit is defined as the number of cycles required (time) change the dynamic response of the beam. In all samples that were fully cured, the associated failure mode in TPB specimens was observed to be core shear failure accompanied with facesheet debonding. When this failure occurs in a vibrating specimen, its stiffness changes and a change in the resonance frequency is immediately observed. The development of the core shear failure in vibrating specimen was observed by the onset of an immediate decrease in the measured resonance displacement. The use of a verified FEA model along with force transducer reading and shaker amplifier input adjustments ensured that the correct stress ratio occurred at the desired area during testing. Figure 4.24 shows and example of core shear failure in the vibrations specimen.

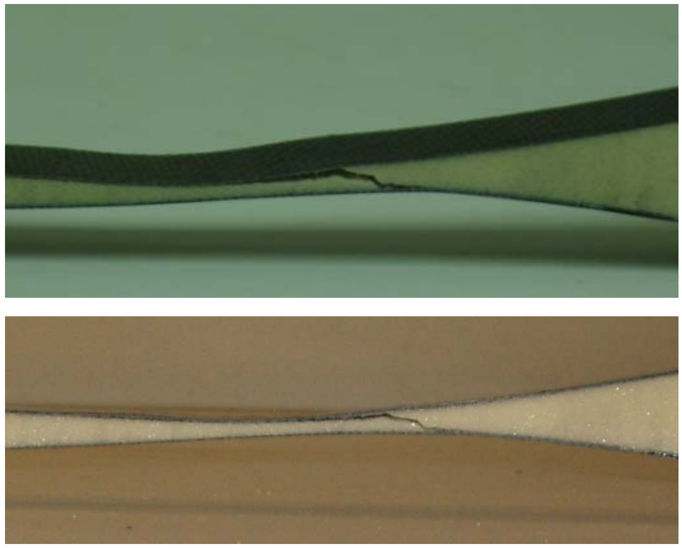

Figure 4.24: Shear core delamination failure occurring in vibration specimens

4.3.2.1 Experimental vibration results

Vibration fatigue analysis was performed until shear core-failure and facesheet delamination occurred. The specimen vibration time was recorded and the number of cycles to failure was determined. Experimental results are shown in Table 4.5.

Table 4.5 Experimental result from Vibration test

Stress Ratio	Experimental Result (Hz)	Predicted Frequency (Hz)	Average cycles to failure
0.77	32.5	31	5954
0.70	31.95	31	18078
0.62	32.25	31	85461
0.55	32.5	31	186876

As with TPB, the vibration fatigue data exhibited an exponential behavior as shown in Figure 4.25. By plotting the data on a semi-log scale, Figure 4.26, a best-fit least square line approximation could be obtained. By calculating the appropriate information from the semi-log graph (example, the slope of the line) an exponential curve could be graphed. See Figure 4.27. It is also interesting to note that the same type of scatter behavior found in TPB is also observed with the vibration technique.

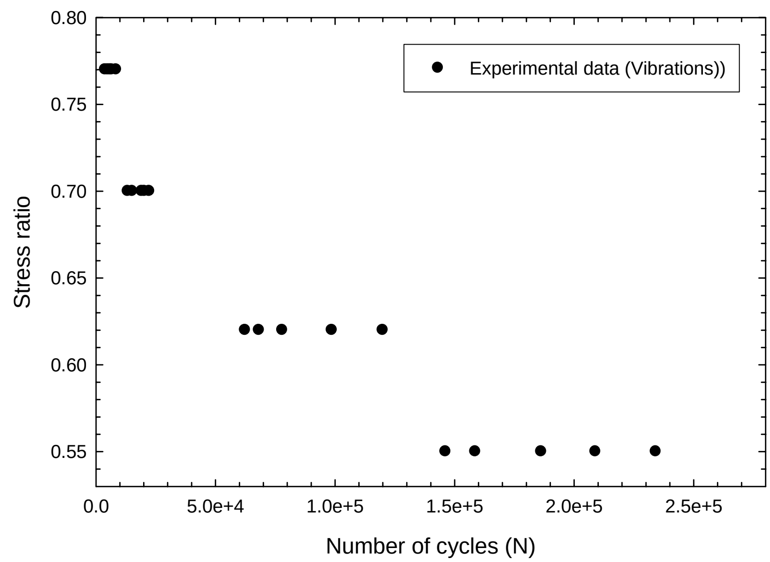

Figure 4.25: Plot lifetime data for composite specimen using vibration methodology

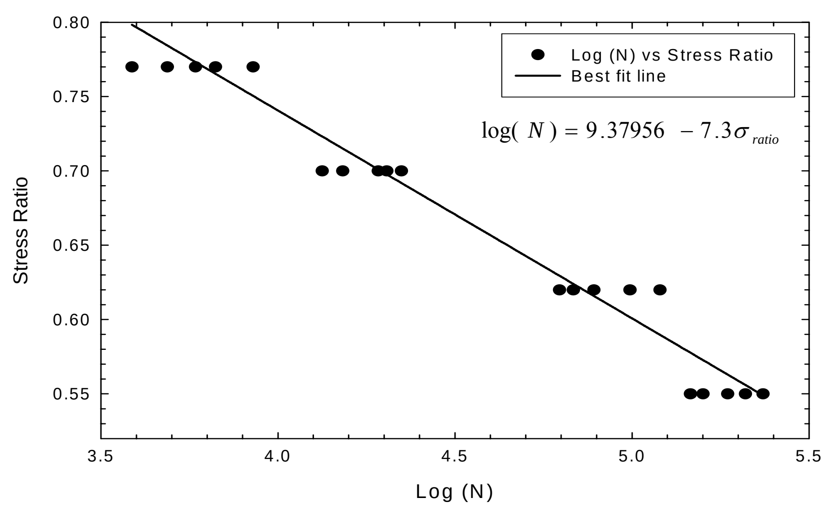

Figure 4.26: Semi-long scale representation of composite specimen vibration

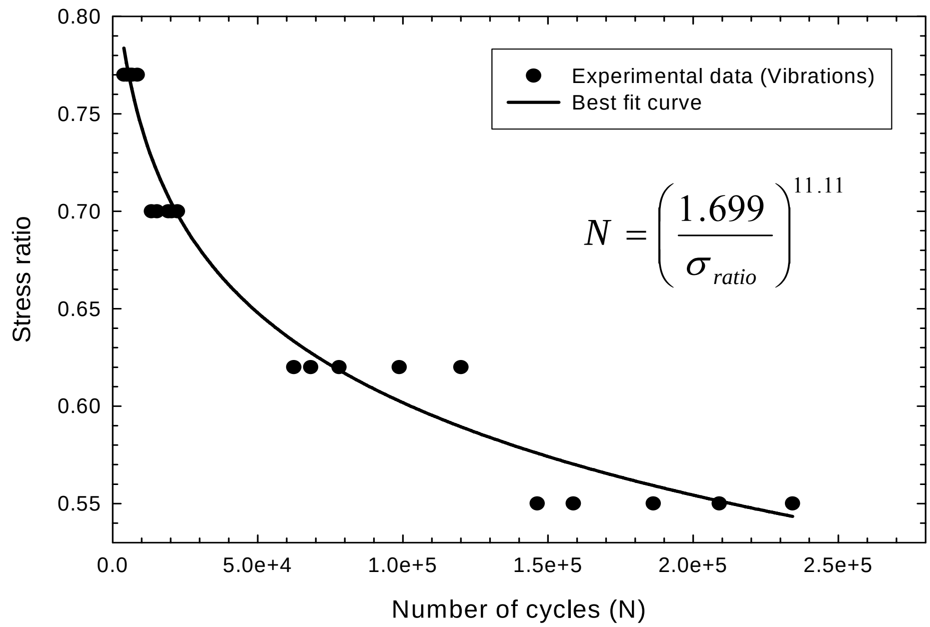

Figure 4.27: Exponential curve approximating lifetime behavior using vibration technique for composite specimen

Table 4.6 shows average number of cycles for each stress ratio obtained through T.P.B. and Vibration testing.

Table 4.6: Comparative results between TPB and Vibrations results

Stress ratio	**Number of cycles (TPB)**	**Number of cycles (Vibrations)**
0.77	4507	5954
0.70	14726	18078
0.62	66741	85461
0.55	166742	186876

4.4 Comparative results of both the Foam and Sandwich Composite

The S-N diagrams of both the FR-7140 foam and sandwich composites samples under TPB and vibration fatigue testing exhibited an exponential behavior. By comparing the data simultaneously, as in Figures 4.28 and 4.29, the accuracy and validity of the procedure can be examined.

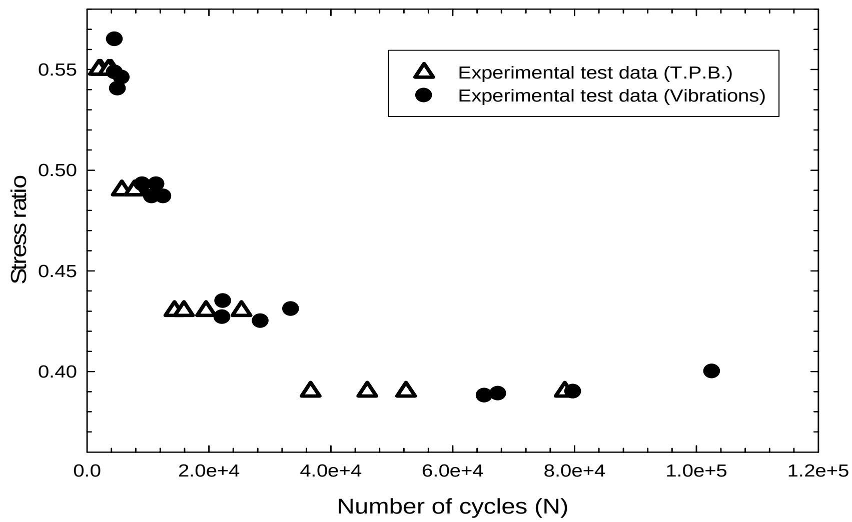

Figure 4.28: Fatigue Lifetime S-N curves for FR7140 foam using both TPB and Vibration fatigue testing.

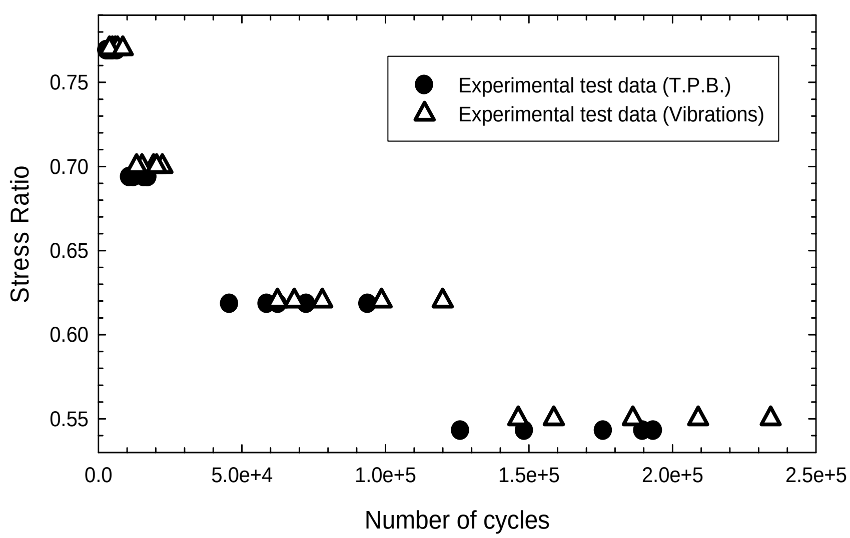

Figure 4.29: Fatigue Lifetime S-N cures for sandwich composites using both TPB and Vibration fatigue testing.

Figures 4.28 and 4.29 clearly show that the results obtained with vibration fatigue are always higher than those from TPB. In addition to this, the scatter observed at the different stress ratios seems to be similar to that found in TPB. In order to help distinguish the effects of the methodology from that of material imperfections both graphs were plotted with their best fit least square lines in a semi-log format as shown in Figures 4.30 and 4.31. It is interesting to note that both material graphs show nearly parallel lines with the vibration technique yielding longer fatigue life predictions for a given stress ratio. By examining Figure 4.4 it is evident that contact between the specimen and testing actuator is always present in TPB testing. This most likely creates contact stresses that influence in the stress life predictions obtained using TPB. Incorporating the contact stress in the Von Misses centerline calculations and transferring these values to the vibration curves can reduce the observed difference.

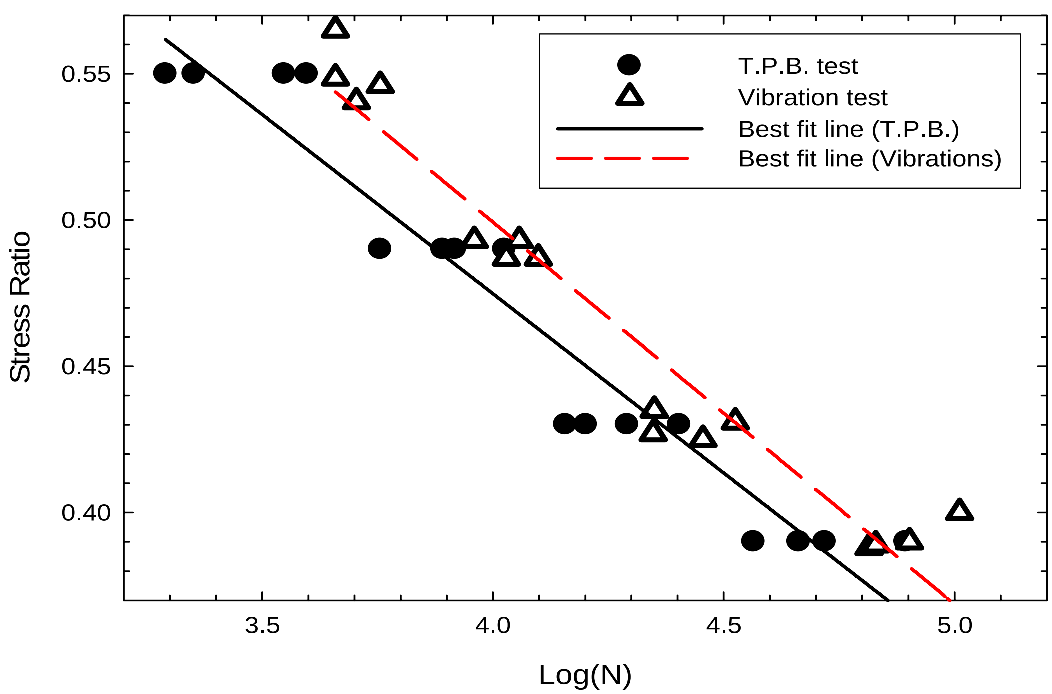

Figure 4.30: FR-7140 S-N semi-log plot for vibration and TPB data

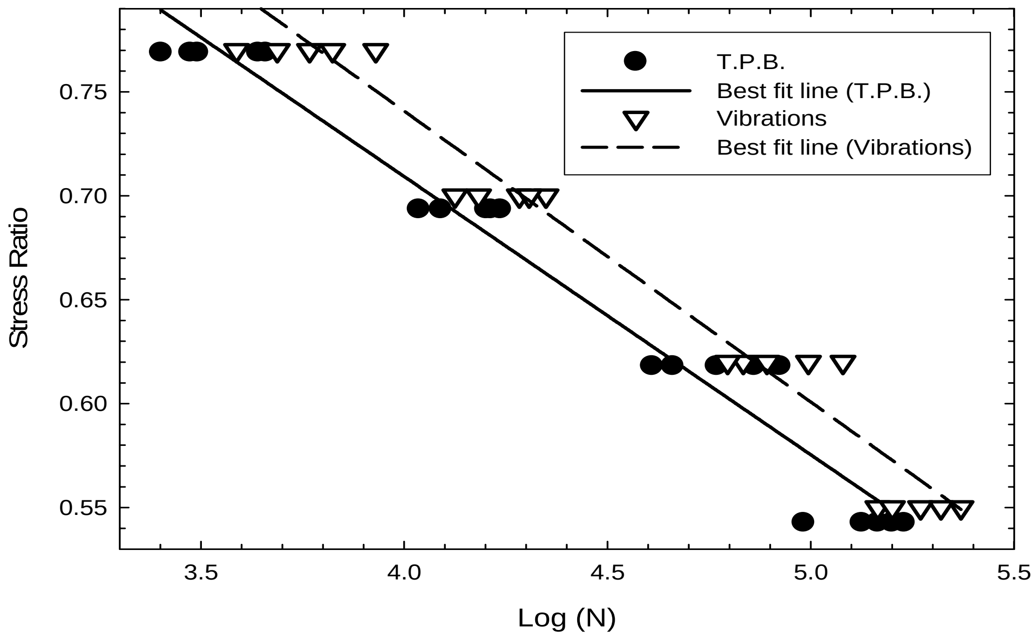

Figure 4.31: Sandwich composite specimen S-N semi-log plot for vibration and TPB data

Figures 4.32 and 4.33 show the TPB exponential curve, the adjusted vibration curve and the vibration curve for the FR7140 foam and sandwich composite respectively.

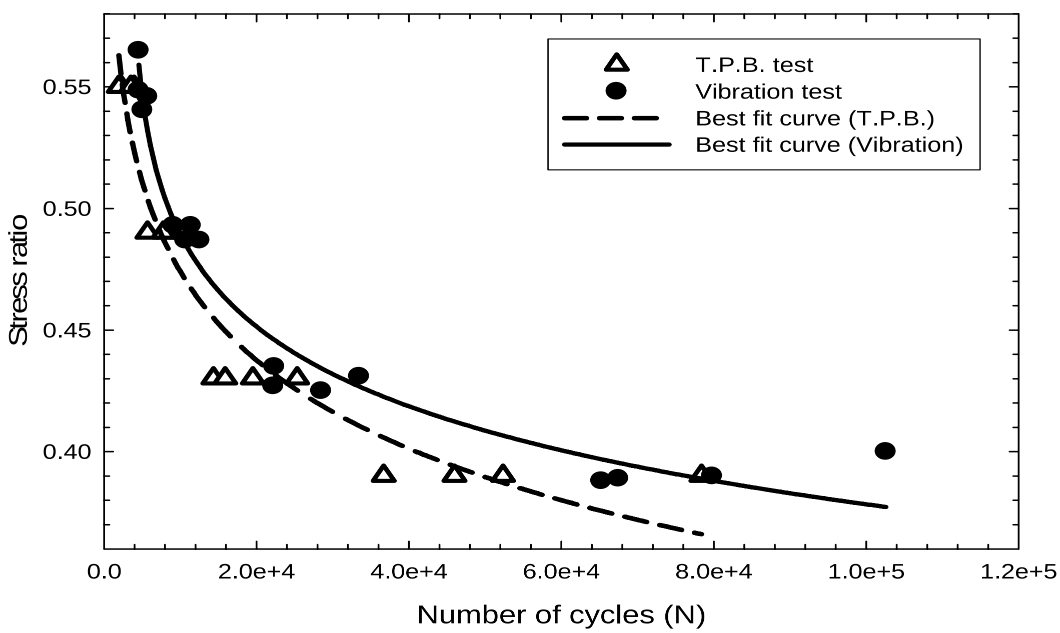

Figure 4.32: Comparison of FR-7140 fatigue life curves (TPB, adjusted vibrations and vibrations).

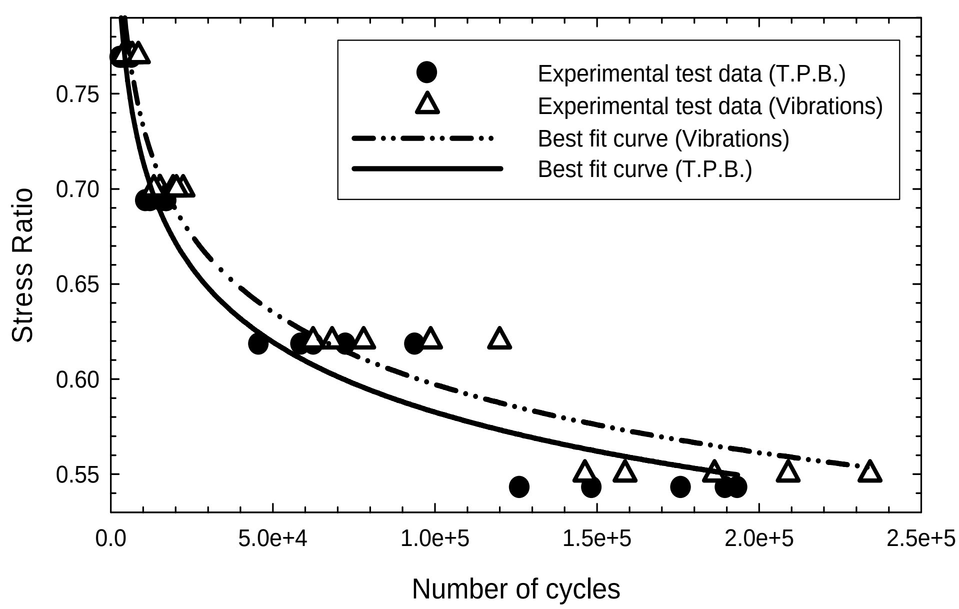

Figure 4.33: Comparison of sandwich composite fatigue life curves (TPB, adjusted vibrations and vibrations).

Graphing the TPB curves with ninety percent confidence intervals further help support the validity of the vibration procedure. Figures 4.34 and 4.35 clearly demonstrate that the error from the vibration technique is well below that of the scatter from material imperfections.

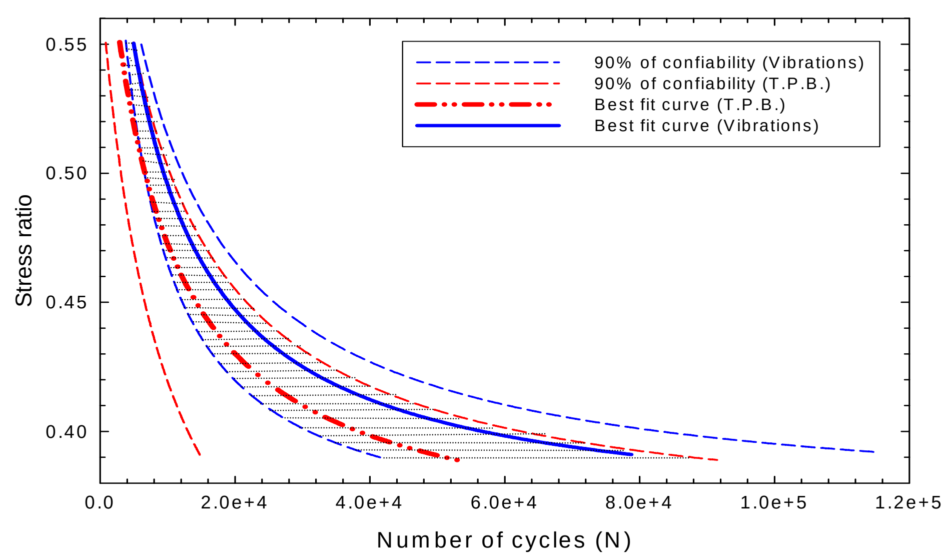

Figure 4.34: FR-7140 TPB fatigue life curve with 90 percent confidence level.

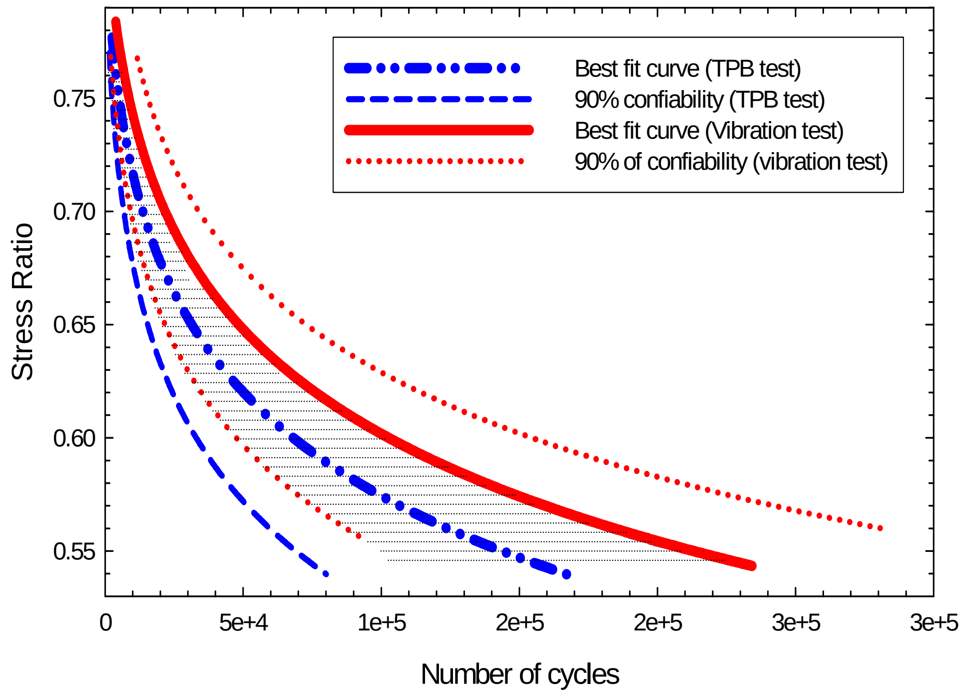

Figure 4.35: Sandwich composite TPB fatigue life curve with 90 percent confidence level.

4.4.1 Contact Stress

It is clearly evident that the fatigue life predicted from vibration testing is higher than that produced by TPB. One possible explanation for this behavior could be attributed to the effect of contact stress encountered in the jig used to hold the TPB specimens. When values are calculated in typical TPB tests, the effect of contact stress is not determined. Thus when compared to TPB these vibration values tend to yield a longer fatigue life. By adjusting for the contact stress, [60, and 61] and considering this in the calculation of the Von-Misses stress, the vibration results can be adjusted. As result of this new consideration the errors between both techniques were reduced considerably, in case of FR-7140 foam from 29% as minimum until -1.25% as minimum and in case of Sandwich Composites from 17% until 1.9% as minimum. Figures 4.36 and 4.37 shows the variation of error over each stress ratio considering contact stress. Finally Figures 4.38 and 4.39 shows the new curves considering contact stresses with additional curves of 90% of confidence.

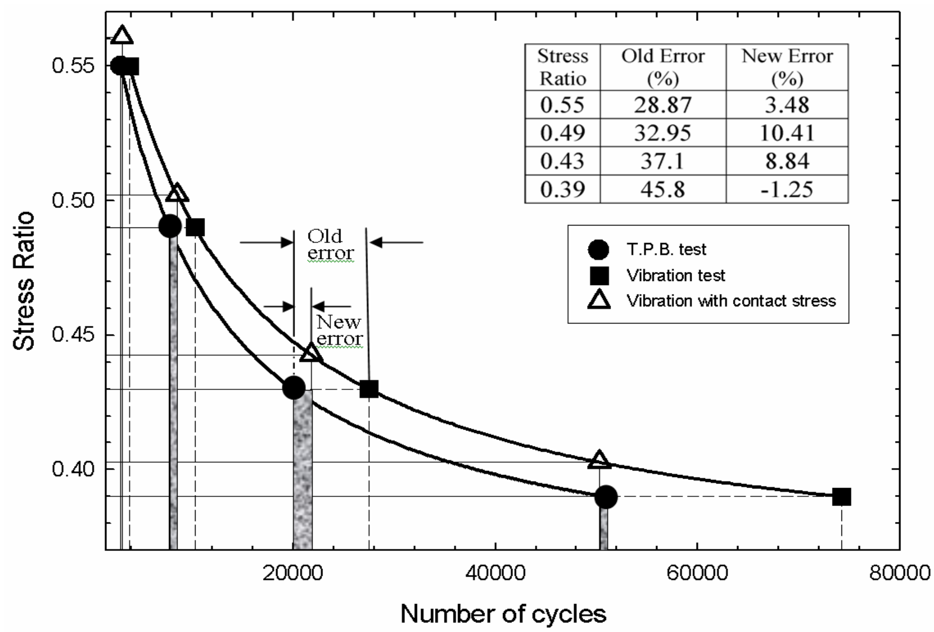

Figure 4.36: Contact stresses and errors in FR-7140 foam

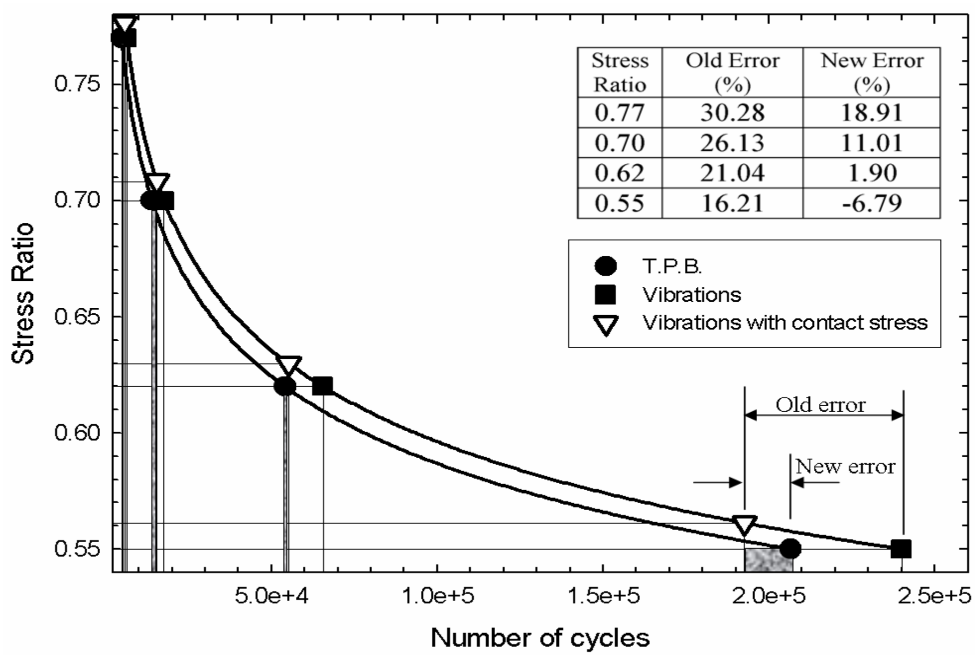

Figure 4.37: Contact stresses and errors in Sandwich Composites

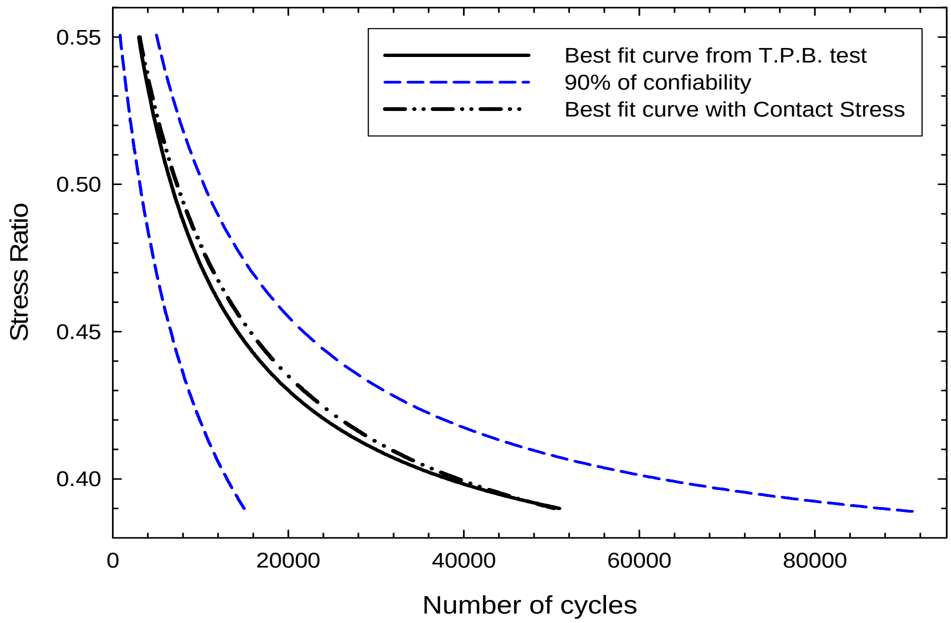

Figure 4.38: Characteristic fatigue curves in FR-7140 foam, considering contact stress

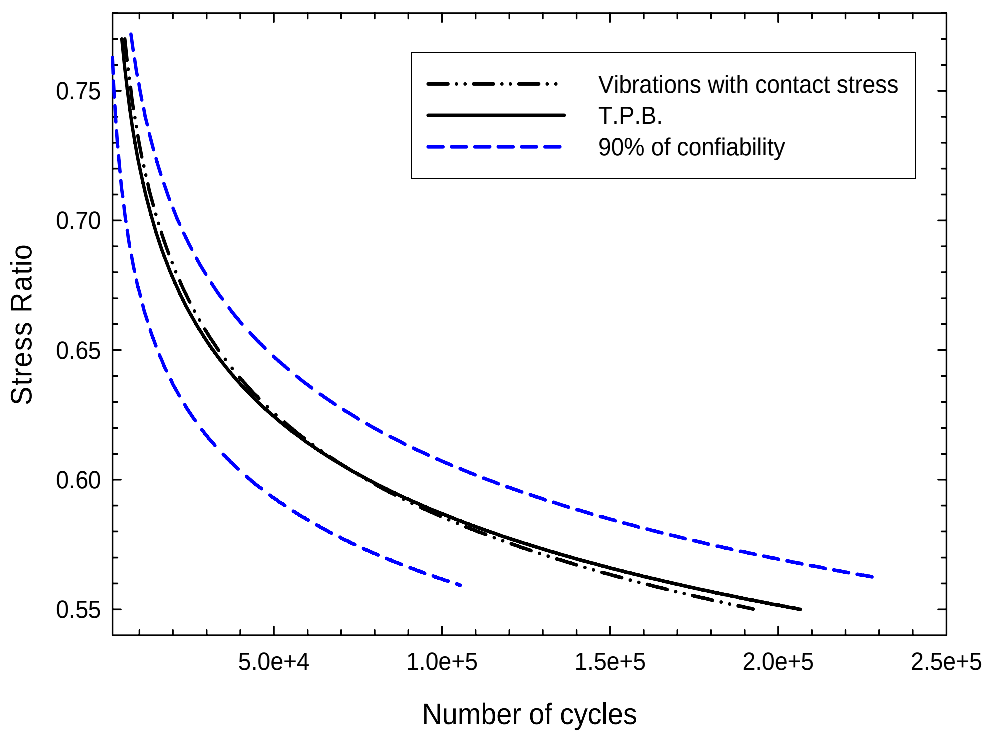

Figure 4.39: Characteristic fatigue curves in Sandwich Composites, considering contact stress

CONCLUSIONS

1. The proposed objective to develop and prove an alternative method using a vibration technique to simulate T.P.B. fatigue testing was developed.

2. This technique was validated using two materials configurations:
    - FR-7140 foam, using sixteen specimens in Vibrations and sixteen specimens to T.P.B.
    - Sandwich composites specimens, using twenty specimens in Vibrations and twenty specimens to T.P.B.

    In all cases fatigue testing was for fully reversed cycles.

3. The time of test using Vibration technique compared with T.P.B. test, was reduced significantly in both cases: 26 times faster in FR-7140 foam and 43 times faster in Sandwich Composites.

4. Analyzing the original result curves of characteristic fatigue life in both cases (FR-7140 foam and Sandwich Composites) always the number of cycles under Vibration test was greater than T.P.B. test, (29% as minimum in FR-7140 foam and 17% as minimum in Sandwich Composites).

5. Considering that T.P.B. specimens generate a contact stress under application of load, and Vibration specimens do not, additional analysis considering the effect of contact stress, and recalculating the Von Misses stress values in the Vibration fatigue curve was performed. This reduces the error between fatigue life curves under Vibrations and T.P.B. significantly. (-1.25% as minimum in FR-7140 foam and 1.9% as minimum in Sandwich Composites).

6. Values of standard deviation seem to be very similar in both methodologies at the same stress ratio. This phenomenon is most likely a characteristic property of the material. The scatter of data increased as the stress ratio decreased.

APENDIX

A. ANALYTICAL MODELING

A one-dimensional Timoshenko beam formulation is developed for a rectangular cantilever beam. In addition, the natural frequencies derived for a cantilever beam from [57] are discussed as a comparative base for future FEA modeling that will be performed on the FR-7140 sandwich beam and sandwich composite.

A.1 Formulation of the problem

Consider a non-uniform beam undergoing transverse vibration, Figure A.1, and a beam element of differential length dx as shown in Figure A.2. Where, $y(x,t)$ is the beam deflection, x is the longitudinal direction, L is the length of the beam, $p(x,t)$ is the forcing function, ψ is the angle of rotation due to bending, β is the angle of distortion due to shear, Q is the shear force, G is the shear modulus of elasticity, M is the moment due to bending.

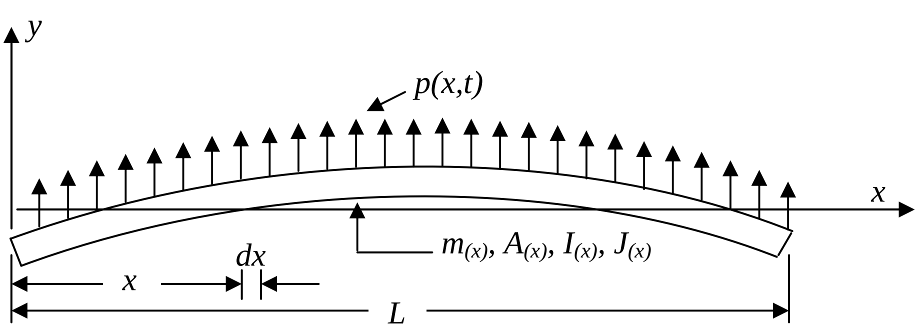

Figure A.1: Timoshenko uniform beam

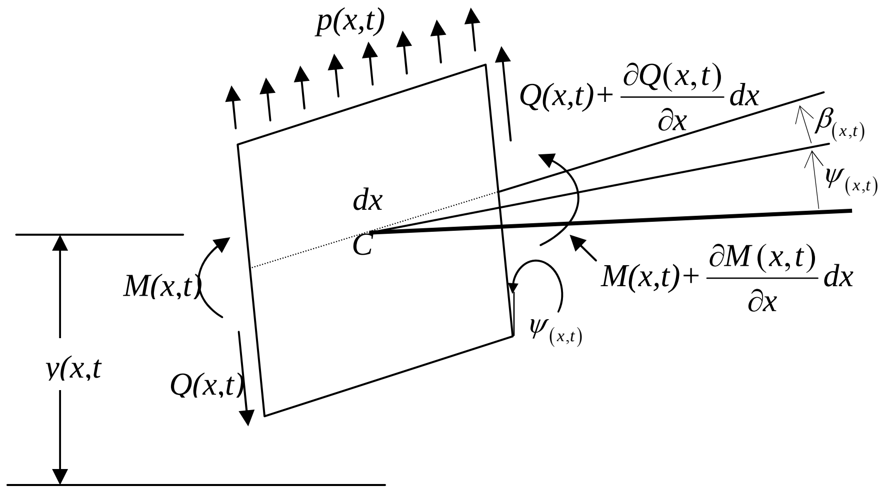

Figure A.2: Timoshenko beam differential element

The total deflection y*(x, t)* at an arbitrary point *x* is caused by the effects of bending and shear and is given in Equation A.1. In addition, the linear and angular deflections are assumed small.

$$\frac{\partial y_{(x,t)}}{\partial x} = \psi_{(x,t)} + \beta_{(x,t)}, \tag{A.1}$$

From mechanics of materials, the relation between the bending moment and bending deformation can be given equation A.2.

$$M(x,t) = EI(x)\frac{\partial \psi(x,t)}{\partial x}, \tag{A.2}$$

Here, E is the Modulus of elasticity and $I\ (x)$ is the Moment of inertia of area about the neutral axis. The relation ship between the shearing force and searing deformation [58], can be given by Equation A.3

$$Q_{(x,t)} = k' G A_{(x)} \beta_{(x,t)}, \tag{A.3}$$

Here G is the shear modulus of elasticity, A is the cross sectional area of the beam and k' is a numerical factor that depends on the cross sectional shape. The governing partial differential equation will be formulated using the extended Hamilton principle, given by Equation A.4. Here T is the kinetic energy and W is the virtual work. The power of this approach becomes evident when we observe that it furnishes automatically the correct number of boundary conditions and their correct expressions.

$$\int_{t1}^{t2} \left(\delta T + \delta W \right) dt = 0 \tag{A.4}$$

The kinetic energy is due to translation and rotation and is expressed by Equation A.5 as

$$T = \frac{1}{2} \int_0^L \left[\frac{\partial y(x,t)}{\partial t} \right]^2 m(x) dx + \frac{1}{2} \int_0^L \left[\frac{\partial \psi(x,t)}{\partial t} \right]^2 J(x) dx. \tag{A.5}$$

Here $m(x)$ is the mass per unit length and $J(x)$ is the mass moment of inertia per unit length about the neutral axis. The mass moment of inertia can be related to the moment of area using the relationship

$$J_{(x)} = \rho I_{(x)} = \frac{m_{(x)}}{A_{(x)}} I_{(x)} = k^2{}_{(x)} m_{(x)}, \tag{A.6}$$

Here k is the radius of gyration about the neural axis and $\rho(x)$ is the mass density of the beam per unit length. The variation of T can be readily written as:

$$\delta T_{(t)} = \int_0^L m \frac{\partial y}{\partial t} \delta\left(\frac{\partial y}{\partial t}\right) dx + \int_0^L k^2 m \frac{\partial \psi}{\partial t} \delta\left(\frac{\partial \psi}{\partial t}\right) dx, \tag{A.7}$$

The virtual work consists of conservative and non-conservative terms and can be express as:

$$\delta W_{(t)} = \delta Wc_{(t)} + \delta Wnc_{(t)} = -\delta V_{(t)} + \int_0^L p_{(x,t)} \delta y_{(x,t)} dx, \tag{A.8}$$

Where the terms W_c, W_{nc} and V are the conservative work, the non-conservative work and the potential energy respectively. Moments and shear cause the beam to bend thus producing potential energy that can be expressed by:

$$V_{(t)} = \frac{1}{2} \int_0^L M_{(x,t)} \frac{\partial \psi_{(x,t)}}{\partial x} dx + \frac{1}{2} \int_0^L Q_{(x,t)} \beta_{(x,t)} dx \tag{A.9}$$

By substituting Equations A.7, A.8 and A.9, into Equation A.4, the following expression given in Equation A.10 is obtained.

$$\begin{aligned} \int_{t1}^{t2} (\delta T + \delta W) dt = \int_{t1}^{t2} \Bigg[& \int_0^L m \frac{\partial y}{\partial t} \delta\left(\frac{\partial y}{\partial t}\right) dx + \int_0^L k^2 m \frac{\partial \psi}{\partial t} \delta\left(\frac{\partial \psi}{\partial t}\right) dx - \int_0^L EI \frac{\partial \psi}{\partial t} \delta\left(\frac{\partial \psi}{\partial t}\right) dx \\ & - \int_0^L k' GA\left(\frac{\partial y}{\partial x} - \psi\right)\left(\frac{\partial y}{\partial x} - \psi\right) dx + \int_0^L p \delta x \delta y \Bigg] dt = 0 \end{aligned} \tag{A.10}$$

Assuming that integration with respect to x and t is interchangeable, the variation and differentiation operators are commutative, and performing integration by parts yields the two arbitrary and independent equations with the following boundary conditions.

$$\frac{\partial}{\partial x}\left[k' GA\left(\frac{\partial y}{\partial x} - \psi\right)\right] - m \frac{\partial^2 y}{\partial t^2} + p = 0 \tag{A.11a}$$

$$\frac{\partial}{\partial x}\left(EI \frac{\partial \psi}{\partial x}\right) + k' GA\left(\frac{\partial y}{\partial x} - \psi\right) - k^2 m \frac{\partial^2 \psi}{\partial t^2} = 0 \tag{A.11b}$$

$$\left(EI\frac{\partial\psi}{\partial x}\right)\delta\psi\bigg|_0^L = 0,\quad \left[k'GA\left(\frac{\partial y}{\partial x}-\psi\right)\right]\delta y\bigg|_0^L = 0 \tag{A.12}$$

Solving Equation A.11b for $\partial\psi/\partial x$ and substituting the result into Equation A.11a, yields the commonly known Timoshenko's equation, Equation A.13, for a uniform beam undergoing forced vibrations.

$$EI\frac{\partial^4 y}{\partial x^4}+\rho A\frac{\partial^2 y}{\partial t^2}-\rho I\left(1+\frac{E}{KG}\right)\frac{\partial^4 y}{\partial x^2\partial t^2}+\frac{\rho^2 I}{KG}\frac{\partial^4 y}{\partial t^4}+\frac{EI}{KAG}\frac{\partial^2 p}{\partial x^2}-\frac{\rho I}{KAG}\frac{\partial^2 p}{\partial t^2}-p=0 \tag{A.13}$$

In free vibrations, *p(x,t)* = 0, and Equation A.13 can be expressed as Equation A.14

$$\rho A\frac{\partial^2 Y}{\partial t^2}-\rho I\frac{\partial^4 Y}{\partial t^2\partial x^2}+EI\frac{\partial^4 Y}{\partial x^4}+\frac{\rho}{KGA}\left(\rho I\frac{\partial^4 Y}{\partial t^4}-EI\frac{\partial^4 Y}{\partial t^2\partial x^2}\right)=0 \tag{A.14}$$

In order to obtain the vibration frequencies of the beam, an eigen-value problem must be formulated. This will be done using the separation of variables method, considering an harmonic movement of the form:

$$Y_{(x,t)}=y_{(x)}\cdot e^{-i\omega t} \tag{A.15}$$

Substituting Equation A.15 into the Timoshenko's beam equation, Equation (A.14), for free vibration, yields Equation A.16.

$$-\rho A\omega^2 y+\rho I\omega^2\frac{\partial^2 y}{\partial x^2}+EI\frac{\partial^4 y}{\partial x^4}+\frac{\rho}{KGA}\omega^2\left(\rho I\omega^2 y+EI\frac{\partial^2 y}{\partial x^2}\right)=0 \tag{A.16}$$

By defining the following non-dimensional parameters

$$\xi=\frac{x}{L},\quad \eta=\frac{y}{L},\quad \phi^2=\frac{\rho AL^4}{EI}\omega^2,\quad \alpha=\frac{EI}{KGAL^2},\quad \beta=\frac{I}{AL^2} \tag{A.17}$$

And replacing these expressions into Equation A.16 yields Equation A.18:

$$\frac{d^4\eta}{d\xi^4}+\phi^2\left(\alpha+\beta\right)\frac{d^2\eta}{d\xi^2}-\phi^2\left(1-\phi^2\alpha\beta\right)\eta=0 \tag{A.18}$$

In this study, we will investigate a cantilever beam whose boundary conditions for Equation A.18 can be given by.

- **Clamped end:**

$$\begin{array}{ll} \textit{Zero displacement} & \eta=0 \\ \textit{Zero rotation} & \dfrac{d\eta}{d\xi}=0 \end{array} \tag{A.19a}$$

- **Free end:**

$$\begin{array}{ll} \textit{Zero moment} & \dfrac{d^2\eta}{d\xi^2}+\phi\alpha\eta=0 \\ \textit{Zero shear effect} & \dfrac{d^3\eta}{d\xi^3}+\phi^2\left(\alpha+\beta\right)\dfrac{d\eta}{d\xi}=0 \end{array} \tag{A.19b}$$

In many applications as assumed here, the effects of rotational inertia can be neglected, $\beta=0$, and Equation A.18 can be reduced to:

$$\frac{d^4\eta}{d\xi^4}+\alpha\phi^2\frac{d^2\eta}{d\xi^2}-\phi^2\eta=0 \tag{A.20}$$

Equation A.20 is a fourth-order differential equation whose characteristic polynomial can be expressed as:

$$P\left(r\right)=r^4+\alpha\phi^2r^2-\phi^2 \tag{A.21}$$

Equation A.21 has 4 roots given by:

$$\begin{aligned} r_1&=-r_2=-i\lambda \\ r_3&=-r_4=-\mu \end{aligned} \tag{A.22}$$

where:

$$\lambda = \sqrt{\frac{1}{2}\alpha\phi^2 + \frac{1}{2}\sqrt{\left(\alpha^2\phi^2 + 4\phi^2\right)}}$$
and
$$\mu = \sqrt{-\frac{1}{2}\alpha\phi^2 + \frac{1}{2}\sqrt{\left(\alpha^2\phi^2 + 4\phi^2\right)}} \tag{A.23}$$

Once the characteristic values of equation 3.20 are obtained, the general solution can be expressed as:

$$\eta(\xi) = A\cos\lambda\xi + B\sin\lambda\xi + Ce^{-\mu\xi} + De^{-\mu(\xi-1)} \tag{A.24}$$

By using the boundary conditions given in Equation A.19 into Equation A.24 produces the following matrix-vector relationship

$$M(\lambda)\begin{bmatrix} A \\ B \\ C \\ D \end{bmatrix} = 0. \tag{A.25}$$

Here $M(\lambda)$ is the matrix given by Equation (A.26)

$$\begin{bmatrix} 1 & 0 & 1 & e^{-\mu} \\ 0 & \lambda & -\mu & \mu e^{-\mu} \\ -\lambda^2\cos\lambda + \phi^2\alpha\cos\lambda & -\lambda^2\sin\lambda + \phi^2\alpha\sin\lambda & \mu^2 e^{-\mu} + \phi^2\alpha e^{-\mu} & \mu^2 + \phi^2\alpha \\ -\lambda^3\sin\lambda - \phi^2\alpha\lambda\sin\lambda & -\lambda^3\cos\lambda + \phi^2\alpha\lambda\cos\lambda & \mu^3 e^{-\mu} - \phi^2\alpha e^{-\mu} & \mu^3\phi^2\alpha\mu \end{bmatrix} = 0 \tag{A.26}$$

In order to obtain a nontrivial solution, the determinant must equal zero thus:

$$f_d(\lambda) = \det M(\lambda) = 0 \tag{A.27}$$

Performing this task and simplifying terms yields:

$$f_d(\lambda) = \mu\lambda\left[\left(\lambda^2 - \mu^2\right)\left(1 - e^{-2\mu}\right)\mu\sin\lambda + \left(1 + e^{-2\mu}\right)2\mu^2\lambda^2\cos\lambda + 2\left(\lambda^4 + \mu^4\right)e^{-\mu}\right] = 0 \tag{A.28}$$

The roots of Equation 3.28 can be expressed by the function:

$$f(\lambda) = \alpha \frac{\lambda^2}{\sqrt{1+\alpha\lambda^2}}\left(1-e^{-2\mu}\right)\sin\lambda + 2\left(1+e^{-2\mu}\right)\cos\lambda + 2\frac{\left(1+\alpha\lambda^2\right)^2+1}{1+\alpha\lambda^2}e^{-\mu} \tag{A.29}$$

$$\left(2n-1\right)\frac{\pi}{2} < \lambda_n < \left(2n+1\right)\frac{\pi}{2}, \quad n = 1,2,3,... \tag{A.30}$$

A more details deduction about the above solution and equations developed can be found in references [57, 58, and 59]

A.2 Numeric application

Consider the example given in the reference [56]. Here an Aluminum beam having a square cross sectional area under a cantilever beam configuration is examined. The physical parameters are given by:

$$K = 1$$
$$\upsilon = 0.33$$
$$E = 714000\ kgf\ /\ cm^2$$
$$G = 268421.05\ kgf\ /\ cm^2$$
$$I = 8333333.33\ cm^4$$
$$A = 10000\ cm^2$$
$$L = 300\ cm^2$$
$$\gamma = 0.00271\ kgf\ /\ cm^3$$
$$G = \frac{E}{2(1+\upsilon)}$$

and the non-dimensional parameters are:

$$\alpha = \frac{EI}{KGAL^2} = 0.0246296$$
$$\beta = \frac{I}{AL^2} = 0.0092593$$

By using Equation A.29 Table A.1 is obtained. A detailed discussion of this is found in [56]. Table A.1 shows a comparison between the first five natural frequencies of a classical Euler-Bernoulli beam and those of the Timoshenko beam developed. This information is quite helpful because it can be used as a base line to validate the FEA that will be used in modeling the FR-7140 foam beam and the sandwich composite.

Table A.1: Comparative results using Euler-Bernoulli and Timoshenko's equation

	1^{st} mode (Hz)	2^{nd} mode (Hz)	3^{rd} mode (Hz)	4^{th} mode (Hz)	5^{th} mode (Hz)
Timoshenko Beam	3.55430	19.01901	42.30733	65.18720	87.79796
Euler - Bernoulli	3.51602	22.03449	61.69721	120.90192	199.85953

B. CONTACT STRESS CALCUALTION

This appendix discusses the methodology used to calculate the effect of the contact stress produced by the holding jig used in T.P.B. The equation [60] used was developed for the contact stress between two rollers and is given by Equation B.1 as:

$$P_o = \left(\frac{P' E^*}{\pi R} \right)^{1/2} . \qquad \text{B.1}$$

Here P_o is the maximum pressure over the specimen, P’ is the applied force per unit length, R is the effective curvature and E^* is the contact modulus. The formulas for determining the effective curvature and contact modulus are given in Equations B.2 and B.3 respectively.

$$\frac{1}{R} = \frac{1}{R_1} + \frac{1}{R_2} \qquad \text{Effective curvature} \qquad \text{B.2}$$

$$\frac{1}{E^*} = \frac{1-\upsilon_1^2}{E_1} + \frac{1-\upsilon_2^2}{E_2} \qquad \text{Contact Modulus} \qquad \text{B.3}$$

Since the jig holds a bar R_2 is assumed infinite because of the flat surface. $R_{1,}$ which is 0.5 inch for this case, is the radius of the damping rubbers placed around the metallic pin used to hold the specimen in the jig. The Modulus of elasticity of the rubber, E_1, is 100 MPa [xx] and E_2 is the Modulus of elasticity of the FR-7140 foam which is 1.127 GPa [xx]. P’ is the applied force per unit length and is calculated in this example as the case corresponding to a applied force of 650 N which represents a stress ratio of 0.55 in the T.P.B. fatigue curve. Considering that the pin holding the specimen is 3.81 cm long, the value of P’ is calculated to be 16250N/m. Using the aforementioned values in Equation B.1 yields a contact stress corresponds to a compression stress of 4.585 MPa. It should be noted that this stress is perpendicular to the surface of the specimen. In order to recalculate the new Von Misses stress value at the surface, the effect of the compressive stress along with the bending stress, which is perpendicular to the contact stress, is taken into account. Once this is performed, the new value was divided by ultimate stress to determine the new stress ratio value, which changed from 0.55 to 0.57. Taking this value and placing it over the vibration fatigue curve yields the new fatigue life value as explained in chapter 4.

REFERENCES

[1] Allen, H.G. "Analysis and Design of Structural Sandwich Panels", Paragon Press,London, (1969).

[2] Zenkert, D. "An Introduction to Sandwich Construction", Chameleon, London (1995).

[3] Daniel, I.M., Gdoutos, E.E., Wang, K.A. and Abbot, J.L. (2002). Failure Modes of Composite Sandwich Beams, International Journal of Damage Mechanics, 11(4): 309–334.

[4] Gdoutos, E.E., Daniel, I.M. and Wang, K.A. (2002). Indentation Failure in Composite Sandwich Structures, Experimental Mechanics, 42(4): 426–431.

[5] Gdoutos, E.E., Daniel, I.M. and Wang, K.A. (2003). Compression Facing Wrinkling of Composite Sandwich Structures, Mechanics of Materials, 35(6): 511–522. Fatigue of Foam and Honeycomb Core Composite Sandwich Structures 315

[6] Steeves, C.A. and Fleck, N.A. (2004). Collapse Mechanisms of Sandwich Beams with Composite Faces and a Foam Core, Loaded in Three-point Bending. Part I: Analytical Models and Minimum Weight Design, International Journal of Mechanical Sciences, 46(4): 561–583.

[7] Steeves, C.A. and Fleck, N.A. (2004). Collapse Mechanisms of Sandwich Beams with Composite Faces and a Foam Core, Loaded in Three-point Bending. Part II: Experimental Investigation and Numerical Modeling, International Journal of Mechanical Sciences, 46(4): 585–608. Figures [10], [11] and [12] reprinted with permission from Elsevier.

[8] Lee, S.M. and Tsotsis, T.K. (2000). Indentation Failure Behavior of Honeycomb Sandwich Panels, Composites Science and Technology, 60(8): 1147–1159.

[9] Pan, S.D., Wu, L.Z., Sun, Y.G., Zhou, Z.G. and Qu, J.L. (2004). Longitudinal Shear Strength and Failure Process of Honeycomb Cores, Composite Structures, 72(1): 42–46.

[10] Petras, A. and Sutcliffe, M.P.F. (1999). Failure Mode Maps for Honeycomb Sandwich Panels, Composite Structures, 44(4): 237–252. Figures [15] and [16] reprinted with permission from Elsevier.

[11] ASTM Standard, C393-62. Standard Test Methods for the Flexural Properties of Flat Sandwich Constructions.

[12] Lim, T.S., Lee, C.S. and Lee, D.G. (2004). Failure Modes of Foam Core Sandwich Beams under Static and Impact Loads, Journal of Composite Materials, 38(18): 1639–1662.

[13] ASTM D 5942 (1999). Determining Charpy Impact Strength of Plastics, American Society of Testing and Materials.
[14] Abrate, S. (1998). Impact on Composite Structures, Cambridge University Press.
[15] Abrate, S. (1997). Localized Impact on Sandwich Structures with Laminated Facing, Applied Mechanics Reviews, 50(2): 83–96.

[16] Todd A. Anderson "An investigation of SDOF models for large mass impact on sandwich composites", Composites Part B: Engineering, Vol. 36, Issue 2, March 2005, pages 135-142

[17] Harte, A.M., Fleck, N.A. and Ashby, M.F. (2001). The Fatigue Strength of Sandwich Beams with an Aluminum Alloy Foam Core, International Journal of Fatigue, 23(6): 499–507.

[18] Kulkarni, N., Mahfuz, H., Melanie, S. and Carlson, L.A. (2004). Fatigue Failure Mechanism and Crack Growth in Foam Core Sandwich Composites under Flexural Loading, Journal of Reinforced Plastics & Composites, 23(1): 83–94.

[19] Gamstedt, E. K. and Sjogren, B.A.(2002).An Experimental Investigation of the Sequence Effect in Block Amplitude Loading of Cross-ply Composite Laminates. International Journal of Fatigue, Vol. 24, Issues 2-4,February-April 2002, Pages 437-446

[20] Clark, S. D., Shenoi, R. A. and Allen, H.G. (1999). Modeling the Fatigue Behavior of Sandwich Beams under Monotonic, 2-step and Block Loading Regimes. Composites Science and Technology, Vol. 59, Issue 4, March 1999, Pages 471-486

[21] Berkowitz, C.K. and Johnson, W.S. (2005). Fracture and Fatigue Tests and Analysis of Composite Sandwich Structure, Journal of Composite Materials, 39(16): 1417–1431.

[22] Erickson, M.D., Kallmeyer, A.R. and Kellogg, K.G. (2005). Effect of Temperature on the Low-velocity Impact Behavior of Composite Sandwich Panels, Journal of Sandwich Structures and Materials, 7(3): 245–264.

[23] Kanny, K., Mahfuz, H., Thomas, T. and Jeelani, S. (2004). Temperature Effects on the Fatigue Behavior of Foam Core Sandwich Structures, Polymers and Polymer Composites, 12(7): 551–559.

[24] Smith, L.V. and Weitsman, Y.J. (1996). The Immersed Fatigue Response of Polymer Composites, International Journal of Fracture, 82(1): 31–42.

[25] Kanny, K. and Mahfuz, H. (2005). Flexural Fatigue Characteristics of Sandwich Structures at Different Loading Frequencies, Composite Structures, 67(4): 403–410.

[26] Burman, M. and Zenkert, D. "Fatigue of Foam Core Sandwich Beams-1:Undamaged Specimens". International Journal of Fatigue, Volume 19. Issue 7, October 1997, pages 551-561.

[27] Burman, M. and Zenkert, D. “Fatigue of Foam Core Sandwich Beams – 2: Effect of Initial Damage”. International Journal of Fatigue, Volume 19. Issue 7, October 1997, pages 563-578.

[28] Sendeckyj, G.P. (1990). Life Prediction for Resin-matrix Composite Materials. In: Reifsnider, K.L. (ed.), Fatigue of Composite Materials, 431–480.

[29] Dai, J. and Hahn, H.T. (2004). Fatigue Analysis of Sandwich Beams using a Wear-out Model, Journal of Composite Materials, 38(7): 581–589.

[30] Reifsnider, K.L., Schulte, K. and Duke, J.C. (1983). Long Term Behavior of Composite Materials, In: Long Term Behavior of Composites, ASTM STP, 813: 136–159.

[31] Wu, W.F., Lee, L.J. and Choy, S.T. (1996) A Study of Fatigue Damage and Fatigue Life of Composite Laminates, Journal of Composite Materials, 30(1): 123–137.

[32] Mahi, El A., Farooq, M.K., Sahraoui, S. and Bezazi, A. (2004). Modeling the Flexural Behavior of Sandwich Composite Materials under Cyclic Fatigue, Materials & Design, 25(3): 199–208.

[33] Palmgren-Miner, M.A. (1945). Cumulative Damage in Fatigue, Journal of Applied Mechanics, 12(3): 159–164.

[34] Hashin, Z. and Rotem, A. (1978). A Cumulative Damage Theory of Fatigue Failure, Journal of Material Science Engineering, 34(2): 147–160.

[35] Wang, A.S.D., Chou, P.C. and Alper, J. (1981). Effect of Proof Test on the Strength and Fatigue Life of a Unidirectional Composite, Fatigue of Fibrous Composite Materials ASTM STP, 723, 116–132.

[36] Broutman, L.J. and Sahu, S.A. (1972). New Theory to Predict Cumulative Fatigue Damage, In: Fiberglass Reinforced Plastics, Composite Materials: Testing and Design (Second Conference), ASTM STP, Vol. 497, pp. 170–188.

[37] Epaarachchi, J.A. and Clausen, P.D. (2005). A New Cumulative Fatigue Damage Model for Fiber Reinforced Plastic Composites under Step/Discrete Loading, composites: Part A, 36(9): 1236–1245.

[38] Sachse, W., Castagnede, B., Grabec, I., Kim, K.Y. and Weaver, R.I. (1990). Recent Developments in Quantitative Ultrasonic NDE of Composites, Ultrasonics **28** (1990), pp. 97–104.

[39] Akay, M. and Hanna, R. (1990). A Comparison of Honeycomb-core and Foam-core Carbon-fibre/Epoxy Sandwich Panels. Composites **21** (1990), pp. 325–331.

[40] Gupta, N. and Sankaran, S. (1999). On the Characterization of Syntactic Foam Core Sandwich Composites for Compressive Properties. Journal of Reinforced Plastics and Composites, Vol. 18, No. 14, 1347-1357 (1999)

[41] Legendre, S., Goyette, J. and Massicott, D. (2001). Ultrasonic NDE of Composite Material Structures using Wavelet Coefficients. Non-Destruct Test Eval Int **34** (2001), pp. 31–37.

[42] Favro, L.D., Jin, H.J., Wang, Y.X., Ahmed, T., Wang, X., Kuo, P.K. and Thomas, R.L. (1993). IR Thermal Wave Tomographic Studies of Structural Composites, In: Thompson, D.O. and Chimenti, D.E., (eds), Review of Progress in Quantitative Nondestructive Evaluation, NDT & E International, 28 Jul.–2 Aug. 1991; Vol. 26(2), p. 99, Plenum Press, Brunswick, Maine (United States) 11A: 447–451.

[43] Favro, L.D., Thomas, R.L., Han, X., Ouyang, Z., Newaz, R.L. and Gentile, G.D. (2001). Sonic Infrared Imaging of Fatigue Cracks, International Journal of Fatigue, 23(Supplement 1): S471–S476.

[44] Guazzone, L.J.-P. and Danjoux, R. (1996). Inspection of New Aeroengine Components by Thermal Wave, NDT & E International, 29(6): 392.

[45] Dattoma, V., Marcuccio, R., Pappalettere, C. and Smith, G.M. (2001). Thermographic Investigation of Sandwich Structure made of Composite Material, NDT AND E International, 34(8): 515–520.

[46] Mandelis, A. (2001). Diffusion-wave Laser Radiometric Diagnostic Quality-control Technologies for Materials, NDE/NDT, NDT & E International, 34(4): 277–287.

[47] Mandelis, A., Munidasa, M. and Nicolaides, L. (1999). Laser Infrared Photothermal Radiometric Depth Profilometry of Steels and its Potential in Rail Track Evaluation, NDT & E International, 32(8): 437–443.

[48] Gibson, R.F. (2000). Modal Vibration Response Measurements for Characterization of Composite Materials and Structures, Composite Science and Technology, 60(15): 2769–2780.

[49] Liew, K.M., Xiang, Y. and Kitiponchai, S. (1995). Research on Thick Plate Vibration: A Literature Survey, Journal of Sound and Vibration, 180(1): 163–176.

[50] Salawu, O.S. (1997). Detection of Structural Damage through Changes in Frequency: A Review, Engineering Structures, 19(9): 718–723.

[51] Palozotto, A.N., Gummadi, L.N.B., Vaidya, U.K. and Herrup, F.J. (1995). Low Velocity Impact Damage Characteristics of Z-fiber Reinforced Sandwich Panels – An Experimental Study, Composites Structures, 43(4): 275–288.

[52] Ayorinde, E.O. (1995). Elastic Constants of Thick Orthotropic Composite Plates, Journal of Composite Materials, 28(8): 1025–1039.

[53] D. Shu “Vibration of Sandwich Beams With Double Delaminations”, Composites Science and Technology, Vol. 54, Issue 1, 1995, pages 101-109.

[54] Tommy J. George, Jeremy Seidt, M. Hernan Shen, Theodore Nicholas, Charles J. Cross, (2003) “Development of a novel Vibration-Based fatigue testing methodology”, International Journal of Ftigue, Volume 26, Issue 5, May 2004, pages 477-486

[55] Jeremy Daniel Seidt, Thesis of “Development of a Novel Vibration Based High Cycle Fatigue Test Method”, The Ohio State University 2001.

[56] O. Scott-Emuakpor, H. Shen, T. George, Ch. J. Cross and J. Calcaterra,” Development of an Improved High Cycle Fatigue Criterion”, Journal of Engineering for gas Turbines and Power, January 2007, Issue 1, 162 (8 pages)

[57] Miguel Angel Moreles y Salvador Botello, “Calculo de frecuencias naturales para vigas elasticas, con efecto de cortante e inercia rotacional. Caso empotrado Articulado”, Rev. Int. Met. Num. Calc. Dis. Ing. Vol 21, 1, 3-21 (2005)

[58] Leonard Meirovitch, “Principles and Techniques of Vibrations”, Four edition, Prentice Hall 1997.

[59] S. Timoshenko, D. H. Young, W. Weaver Jr. “Vibration Problems in Engineering”, John Wiley & Sons, 1974

[60] Jack A. Collins, Failure of Materials in Mechanical Design, Second Edition 1993